



Hydrogen defects in feldspars: defect properties and implications for water solubility in feldspar

Harald Behrens¹

Received: 3 September 2020 / Accepted: 29 November 2020 / Published online: 18 January 2021
© The Author(s) 2021

Abstract

Hydrogen defects can strongly affect mechanical and chemical properties of feldspars. To get insight into the behavior of such defects, alkali feldspar and plagioclase of igneous origin were studied combining IR spectroscopy with heating experiments under well-controlled conditions. Near-infrared spectra show that OH groups are the predominant hydrous species in these feldspars but presence of minor amounts of molecular H₂O cannot be excluded. Short-term annealing at 400–800 °C produces a small but significant irreversible change in the OH stretching vibration band which is attributed to relaxation of the feldspar structure. Polarized mid-infrared spectra of sanidine, adularia, and plagioclase recorded in situ at temperatures up to 600 °C show reversible shifts of maxima toward higher wavenumber and an overall decrease in integrated intensities. The pleochroic features of the OH vibration bands, i.e., the predominant orientation of OH dipoles along the crystallographic *a* axis in all feldspars and the additional band component perpendicular to the (010) plane in sanidine are still present in the high-temperature spectra. Different behavior during long-term annealing at high temperature was found for the alkali feldspars and the plagioclases. At 900–1000 °C, the Eifel sanidines rapidly lost about one quarter of the initial water content which is attributed to a weakly bound hydrogen species in the feldspar structure. The remaining hydrogen is very strongly bound and was still detectable in 0.7–0.9 mm thick sections after annealing for 108 days at 1000 °C in air dried by phosphorus pentoxide. In contrast, a 1-mm-thick section of plagioclase completely lost hydrogen during heating in air within 8 days at 1000 °C. After partial dehydration, the pleochroic behavior of the OH absorption bands of the feldspars was basically preserved except that the 3050 cm⁻¹ band of the sanidine, oriented perpendicular to (010), becomes more pronounced than the 3400 cm⁻¹ band, oriented parallel to the *a* direction. Annealing experiments at 1000 °C under controlled water pressures indicate equilibrium solubilities of several tens of ppm H₂O in the plagioclases and more than 100 ppm H₂O in the alkali feldspars already at 1 bar water pressure. The variation of the water content with H₂O pressure and spectroscopic observations indicates that the water content in the feldspars is determined not only by the water pressure but also by already existing defects. Vacancies on alkali sites (*V*_{Al1}) may accommodate H₂O molecules, possibly with subsequent hydrolysis of network bonds to minimize local stress. A likely explanation for the strongly bound hydrogen in the sanidine is a coupled substitution of H⁺ + Al³⁺ for Si⁴⁺ (AlOH defect) where the protons are located on interstitial sites. This incorporation model is supported by the complete recovery of the defects in H₂O vapor after previous proton/alkali exchange in alkali chloride vapor at 1000 °C.

Keywords Igneous feldspar · Hydrogen defects · Infrared spectroscopy · Water solubility · Diffusion

Supplementary Information The online version contains supplementary material available at <https://doi.org/10.1007/s00269-020-01128-0>.

✉ Harald Behrens
h.behrens@mineralogie.uni-hannover.de

¹ Institut Für Mineralogie, Universität Hannover, Callinstr. 3, 30167 Hannover, Germany

Introduction

Feldspar is the most abundant mineral in the earth's crust. Knowledge on its kinetic behavior can be helpful for understanding and modeling of rock formation and rock deformation. It is well established that intracrystalline processes in feldspar can be strongly enhanced by dissolved hydrogen species. The rates of Al-Si ordering–disordering in alkali feldspars (Yund and Tullis 1980; Goldsmith 1986, 1987, 1988), oxygen isotope exchange between alkali feldspars and

hydrous fluids (Yund and Anderson 1974; Giletti et al. 1978; Elphick et al. 1988; Farver and Yund 1990) and NaSi–CaAl interdiffusion in plagioclase feldspars (Grove et al. 1984; Yund 1986; Baschek und Johannes 1995) are accelerated by several orders of magnitude at elevated water pressures. Strong effects of water on deformation of feldspar minerals or aggregates are evident from several studies (see review of Kohlstedt 2006). Electrical conductivity in plagioclase is also enhanced by hydrogen species, probably by contributions of protons to the charge transport (Yang et al. 2012). Furthermore, hydrogen contents in the nominally anhydrous mineral feldspar have found attraction as possible hygrometer for magmas in terrestrial volcanic rocks (Seaman et al. 2006; Hamada et al. 2011, 2013) and in lunar rocks (Hui et al. 2013; Mills et al. 2017).

Based on infrared spectroscopy, Johnson and Rossman (2004) distinguished different types of structural hydrous species (in this paper, the general term “hydrogen defects” is preferred to include H-bearing defects that do not originate from incorporation of H₂O). Most common in igneous feldspars are defects of type IIa OH which are characterized by very broad IR-absorption bands centered around 3400 cm⁻¹ with the maximum intensity closely aligned with the crystallographic *a* axis. Plagioclase other than low albite contain this type of OH, but it can be found also in alkali feldspars. Defects of type IIb OH are characterized by an additional band at 3050 cm⁻¹ which is most intense in the direction perpendicular to (010). This type of OH band is apparently restricted to sanidine.

Igneous feldspars may contain structural OH (0–512 ppm H₂O), molecular H₂O (0–1350 ppm H₂O), and NH⁴⁺ groups (0–1500 ppm NH⁴⁺) as well as fluid inclusions and alteration products (Johnson and Rossman 2004). Although composition and structure of feldspars do influence the type of hydrogen species, the concentration of these species is not controlled by major-element composition. This conclusion is corroborated by the experimental study of Yang (2012). He observed a systematic increase of the solubility of water in feldspars with pressure and temperature but no correlation with main or trace elements was found.

Hydrogen species identified by infrared spectroscopy in minerals at ambient conditions are not necessarily those that control the kinetic processes (Kronenberg et al. 1996). In volcanic feldspars ejected rapidly during an eruption, the hydrogen defects have been incorporated during crystal growth, possibly in combination with other defects. An example for such kind of incorporation is the substitution of Si⁴⁺ by Al³⁺ on a tetrahedral site and an associated incorporation of a proton on an interstitial site. Such substitution mechanisms will be determined by the activities of the involved components (here SiO₂, Al₂O₃, and H₂O) in the magma. Thus, type and concentration of the hydrogen defects represent specific conditions in the magma chamber

but are not exclusively determined by the water activity in the magma. In other words, the measured hydrogen content in feldspars does not necessarily represent the water solubility in the minerals. Here, the term water solubility refers to the equilibrium between a mineral and a pure H₂O fluid.

Although it has been widely accepted that new defects are formed within the feldspars by interaction with water at high pressure, the nature of the defects and the rate-controlling steps of the water-enhanced kinetic processes are still poorly understood. Different mechanisms have been proposed to explain the effect of hydrogen and water pressure on kinetic properties of feldspars. Buffered experiments have shown that the Al–Si exchange between the tetrahedral sites of feldspars depends on the fugacity of hydrogen, f_{H_2} (Goldsmith 1986, 1987, 1988), and it has been suggested that the thermodynamic variable controlling these processes is the activity of protons, a_{H^+} (Graham and Elphick 1991; Goldsmith 1991). In line with these ideas, Kronenberg et al. (1996, 1998) explained the fast dehydration kinetics of an adularia by a high mobility of protons in the feldspar structure. However, rapid diffusion of H₂O molecules or hydronium cations may be an alternative explanation, as suggested by Doremus (1998).

Oxygen exchange rates in alkali feldspars were found by Farver and Yund (1990) to be directly related to the fugacity of water, $f_{\text{H}_2\text{O}}$. A theory was developed to explain the rapid exchange of oxygen isotopes by diffusion of H₂O as carrier molecules (Zhang et al. 1991). The predominant role of water in oxygen isotope exchange under hydrothermal conditions has been supported by ab initio calculations for another framework silicate, quartz, by McConnell (1995). The theoretical approach proposed by Zhang et al. (1991) was confirmed experimentally for hydrous rhyolitic glass melts using combined hydrogen and oxygen isotope exchange experiments (Behrens et al. 2007). Evidence is also given from laboratory studies that NaSi–CaAl interdiffusion in plagioclase feldspars is directly related to $f_{\text{H}_2\text{O}}$ by homogenization experiments with peristerites using H₂O–N₂ fluid mixtures (Baschek and Johannes 1995).

The present paper is part of an extended experimental study aimed to investigate the nature of hydrogen defects in feldspars, i.e., the high-temperature stability and the mobility of the defects. The study is focused on volcanic feldspars because these feldspars show relatively simple hydrogen defects (Johnson and Rossman 2004) and because large crystals of gem quality are available for diffusion and solubility experiments. The latter constrain is particularly important to investigate volume properties, i.e., to avoid any influence of grain boundaries, pores, inclusions or other extended defects. Most of the experiments were done on sanidines from the Eifel/Germany since these feldspars are already well characterized by a couple of studies (Beran 1986; Bernotat-Wulf et al. 1988; Petrov and Hafner 1988;

Widder et al. 1994; Freer et al. 1997; Derdau et al. 1998; Johnson and Rossman, 2003, 2004). An adularia is used to probe whether the findings on Eifel sanidine are transferable to other K-feldspars. To enlarge the compositional and structural range, plagioclase of labradorite composition is used, for which information on structural and kinetic properties is also available (e.g., Behrens et al. 1990; Johnson and Rossman, 2003, 2004; Yang 2012). It is emphasized that the findings of this study may be not directly transferable to metamorphic feldspars, in which incorporation of hydrogen defects is usually kinetically controlled and hydrogen defects are instable at high temperature (magmatic conditions) (Aines and Rossman 1985; Kronenberg et al. 1996).

The focus of the present paper is on the thermal stability of hydrogen defects in feldspar. Short-term heating experiments at temperatures up to 800 °C with subsequent IR measurements at room temperature as well as in situ IR spectroscopy on feldspar sections at temperatures up to 600 °C give insight to temperature-induced changes in hydrogen positions and bonding. Long-term annealing experiments at controlled temperature, pressure, and water fugacity allow conclusions about the role of intrinsic (controlled only by $p, T, f_{\text{H}_2\text{O}}, f_{\text{O}_2}$) and extrinsic (affected by pre-existing defects in the minerals) hydrogen defects with regard to water solubility in feldspars.

Samples

Volcanic feldspars with the two most frequent hydrogen defects were selected for the investigations. Two sanidines from the Eifel, Germany (labeled SV and S2) and one adularia from an unknown locality (labeled A1) were used as well as three plagioclases from different localities in North America. An additional Eifel sanidine (S3) was not used in experiments but for the quantification of hydrogen contents, i.e., to check calibrations of IR spectroscopy. All feldspars are of gemstone quality with pronounced cleavages parallel to (010) and (001).

Large parts of the crystals are free of cracks and other visible imperfections (e.g., inclusions). The sanidine S2 and the adularia are colorless, and the sanidine SV is smoky colored. Smoky color of Eifel sanidine has been attributed to radiation defects (Speit and Lehmann 1982). After heating above 200 °C, the radiation defects are destroyed, and the crystal is bleached without losing dissolved H₂O, as indicated by IR measurements. Sanidine from Volkesfeld is well characterized by X-ray and optical techniques (e.g., Bertelmann et al. 1985; Fehlmann and Bertelmann 1988; Widder et al. 1994) and by IR, optical absorption, and EPR spectroscopy (Speit and Lehmann 1982; Hofmeister and Rossman 1984, 1985; Beran 1986; Petrov and Hafner 1988; Johnson and Rossman 2003). The highly perfect structure of the sanidine crystals

even in large volumes up to several cm³ was demonstrated by X-ray topography (Widder et al. 1994). Plagioclase crystals are transparent with yellow color due to trivalent iron (Hofmeister and Rossman 1984).

Experimental and analytics

The crystals were oriented and cut parallel to the main cleavage planes (001) and (010). The crystallographic *a*-axis could be easily identified as the intersection of (010) and (001), and some sections were also prepared perpendicular to the *a*-axis. In the case of the adularia, a confirmation of the orientation of crystallographic axis was given by single crystal X-ray measurements and by conoscopic observations (G. Baschek, personal communication). The pleochroisms of the OH absorption bands for sanidine and plagioclase agree well with determinations on similar materials in previous studies (Hofmeister and Rossman 1985; Beran 1986), supporting the accuracy of sample orientation.

Major oxide components were determined by electron microprobe analysis (Table 1) using a Cameca Camebax for alkali feldspars and a Cameca SX100 for plagioclase. Based on the An-content, the plagioclases are classified as labradorite. Alkali feldspars are potassium-rich with iron and barium being major impurities. Noticeable amounts of iron are also dissolved in the plagioclase. As shown in previous studies (Hofmeister and Rossman 1984; Petrov and Hafner 1988) by optical spectroscopy and electron paramagnetic resonance (EPR), all iron is incorporated as Fe³⁺ in potassium-rich alkali feldspars, substituting aluminum on tetrahedral sites. On the other hand, calcium-rich plagioclase formed in volcanic settings may contain both ferrous and ferric iron. According to Hofmeister and Rossman (1984), ferric iron is slightly predominant in labradorite from Lake County with Fe²⁺/Fe³⁺ = 1: 2. However, the location of iron species in the plagioclase structure has not been finally resolved, in particular for ferrous iron. Interpretation of spectroscopic and experimental data has been controversial with assignment of Fe²⁺ to tetrahedral sites, to Ca²⁺ sites or to both (Appleman et al. 1971; Hofmeister and Rossman 1984, 1985). Based on the easy oxidation of Fe²⁺ by annealing in air, Behrens et al. (1990) concluded that ferrous iron cannot be located on a Ca²⁺ site. Absorption spectra recorded in the near infrared and visible range using a Bruker IFS88 spectrometer as well as total iron contents measured by electron microprobe (Table 1) are in good agreement with findings of Hofmeister and Rossman (1984, 1985) for similar feldspars.

Hydrogen contents of feldspars were measured by pyrolysis and subsequent Karl–Fischer titration (KFT), by nuclear reaction analyses (NRA) and by infrared spectroscopy.

Table 1 Composition and density of studied feldspars

	Sanidine SV, Volkesfeld, Eifel, Germany	Sanidine S2, Eifel, Ger- many	Sanidine S3, Eifel, Ger- many	Adularia A1, Unknown locality	Labradorite P8, New Mexico, USA	Labradorite P6, Lake County, Oregon, USA	Labradorite G2, Sonora, Mexico
wt% oxides							
SiO ₂	64.11	64.38		63.85	52.96	51.29	51.31
Al ₂ O ₃	18.71	18.80		18.82	29.26	30.56	30.59
Fe ₂ O ₃	0.17	0.18		0.21	0.37	0.49	0.41
CaO	<0.01	<0.01		<0.01	12.49	13.77	13.52
SrO	0.02	0.04		0.02	0.20	0.08	0.13
BaO	0.61	0.61		1.14	0.06	0.00	0.06
Na ₂ O	1.73	1.73		3.12	4.33	3.73	3.73
K ₂ O	14.48	14.53		12.36	0.34	0.11	0.22
Total	99.83	100.27		99.52	100.03	100.05	99.99
mol% feldspar components							
Ab	15.2	15.2		27.2	37.8	32.7	32.8
Or	83.7	83.8		70.8	2.0	0.6	1.3
An	0.0	0.0		0.0	60.2	66.7	65.8
Ce	1.1	1.1		2.0	0.1	0.0	0.1
ppm H ₂ O (NRA)			197 ± 36				130 ± 43
			186 ± 48				
ppm (H ₂ O) (IR) ^a	129 ± 10	147 ± 8	125 ± 9	128 ± 9	58 ^c	0	124 ± 15
ppm (H ₂ O) (IR) ^b	92 ± 10	105 ± 11	89 ± 10	69 ± 10			67 ± 7
Density (g/l)	2560 ± 15	2537 ± 5		2549 ± 5			2685 ± 10

Density was determined using the buoyancy method, i.e., measuring the weight in water and in air

ppm (NRA) was determined by nuclear reaction analyses at BAM, Berlin. 2σ error obtained from depth profiling are reported

Ab NaAlSi₃O₈, Or KAlSi₃O₈, An CaAl₂Si₂O₈, Ce BaAl₂Si₂O₈

^appm (IR) determined using the absorption coefficient of 107,000 L mol(H₂O)⁻¹ cm⁻² from Johnson and Rossman (2003)

^bppm (IR) determined using the absorption coefficient of 150,000 L mol(H₂O)⁻¹ cm⁻² for sanidine and 202,600 L mol(H₂O)⁻¹ cm⁻² for plagioclase and adularia from Mosenfelder et al. (2015)

^cH₂O content was estimated using a partially polarized IR beam and comparing the peak area to the G2 plagioclase

Karl–Fischer titration

The H₂O content of sanidine SV and plagioclase G2 was measured by Karl–Fischer titration (KFT, see Behrens et al. (1996) for description of the method) using powdered material with grain size < 60 μm. To remove water adsorbed on the surfaces of feldspar grains, samples were pre-annealed at 180–350 °C within the KFT apparatus while purging the apparatus with dry argon. Already during 5-min flushing, the titration rate dropped to the initial (blank) value. After this pre-drying, the sample was heated to 1200 °C within 3 min and kept at this temperature for 5 min. The water released in the temperature interval of 400–1200 °C is assumed to represent the water dissolved in the feldspar. Annealing for longer times gave no measurable increase of the detected water.

It is noteworthy that the feldspars were still grainy after KFT analysis and did not transform into a melt droplet. Hence, in contrast to analysis of glasses (Behrens et al.

1996), the diffusion distance for water in the condensed material remained short, and H₂O could be efficiently extracted. However, it cannot be excluded that a minor portion of H₂O remains in the feldspar grains after the analytical procedure, in particular in the sanidine where some of the hydrogen is strongly bonded (see below).

Nine measurements using 32–276 mg of sanidine SV yield H₂O contents from 200 to 335 ppm by weight. Six analyses using between 80 and 420 mg of plagioclase G2 vary between 100 and 220 ppm H₂O. Analytical error based on uncertainty in titration rate of ± 0.02 μg/s (Behrens 1995) is ± 6 μg for these analyses which corresponds to a precision ± 30 ppm for 200 mg sample. The measured H₂O content for the Eifel sanidine is in good agreement with previous determinations using hydrogen manometry (170 ppm, Hofmeister and Rossman 1985), elementary analysis (360 ppm, Beran 1986), ¹H MAS NMR spectroscopy (170 ppm, Johnson and Rossman 2003) and secondary ion mass spectrometry (102 ppm, Mosenfelder et al.

2015). Although the KFT data are consistent with previous measurements, these data are not included in Table 1 as the precision of this bulk extraction method is less than that of the other methods. An important result of the KFT measurements is that hydrogen is released in the form of H₂O since the analytical method is based on a specific reaction (H₂O + SO₂ + I₂ = SO₃ + 2 HI, Behrens 1995). Therefore, the terms water content and water solubility are used throughout this paper for quantification.

Nuclear reaction analysis (NRA)

The second method applied to determine the absolute quantity of hydrogen in feldspars relies on the nuclear reaction ¹H(¹⁵N, αγ)¹²C (see Rossman 2006). The reaction cross section has a narrow resonance for 6.385 meV. The initially formed unstable ¹⁶O nucleus decays by the emission of an α-particle to an excited ¹²C-nucleus, which subsequently emits 4.43 meV γ-radiation. These γ-rays are detected with an energy-dispersive spectrometer system. The number of measured 4.43 meV-photons is proportional to the hydrogen concentration in the sample material. Due to the high γ-energy, the background in the spectral region of interest is only caused by cosmic radiation.

The sharp resonance in the reaction probability allows profiling of the hydrogen atoms up to a depth of about 2 μm. ¹⁵N ions with an initial energy above the resonance energy are continuously slowed down while penetrating the material. Therefore, by variation of the initial ¹⁵N energy, the H concentration is measured as a function of depth within the material.

NRA of polished crystal plates with ca. 1 × 1 cm area were performed by Dr. U Reinholz at Federal Institute for Materials Research and Testing (BAM) in Berlin. A high-purity polyimide (Kapton C₂₂H₁₀N₂O₅, Dupont company) was used as a standard.

Infrared spectroscopy

IR absorption spectra were recorded using a FTIR spectrometer Bruker IFS88 equipped with an IR microscope A590. In the mid-infrared, a global source and a KBr beamsplitter were applied, and 50–100 scans were accumulated for each spectrum with a spectral resolution of 2 cm⁻¹. The spectrometer provides a partial polarized beam which was used to monitor changes in the water content of samples from solubility experiments. During these measurements, it was ensured that the samples always had the same orientation to the IR beam. Macroscopic measurements on crystal plates were performed within the spectrometer using an MCT detector. Here, the sample was mounted on an aperture hole with 1–4 mm in diameter which selected exclusively the central region of the sample. Measurements with the

IR microscope (equipped with a narrow range MCT detector) were performed using a circular aperture of 0.75 mm in diameter corresponding to a focus diameter of 50 μm.

Polarized spectra in the mid-infrared were measured with the IR microscope using an IR polarizer KRS-5 (Bruker). This technique was applied to characterize the pleochroism of the fundamental OH absorption bands in the starting crystals and in some run products. Furthermore, these spectra allow IR spectroscopic quantification of the water content of the feldspars (Johnson and Rossman 2003).

To distinguish OH groups and H₂O molecules, near-infrared spectra of thick sections were recorded in the spectrometer using a tungsten light source, a CaF₂ beam splitter, and an InSb detector. Here, a partial polarized beam was used to improve the signal to noise ratio, and 100 scans were accumulated with a spectral resolution of 4 cm⁻¹.

Heating experiments

The instantaneous response of hydrogen species upon temperature changes was tested by heating samples at temperatures up to 800 °C for a few minutes and subsequent IR measurements at room temperature. Furthermore, IR absorption spectra were recorded in situ in the IR microscope at temperatures up to 600 °C using a heating stage Linkam THM600 controlled by a programmer Linkam PR600.

To probe the long-term stability of hydrogen defects, different devices were used, depending on desired temperature, pressure and water fugacity. Often, samples with different water content were combined in an experiment to bracket the equilibrium water content for the applied conditions. Conditions and results are summarized in Tables 2, details are given in Tables S1 and S2 in the supplement.

A large set of experiments was performed at ambient total pressure and the water pressure was adjusted with a thermostat via the equilibrium of steam with liquid water. Very low water pressures were established using salt-saturated (LiCl or NaI was added) aqueous solutions or via the ice/water equilibrium. In most cases, a static setup was employed. Samples were placed in a platinum boat on a magnetically movable sample holder and could be rapidly moved in and out of the hot zone of the furnace. Glass components inside the furnace consisted of silica glass.

To test whether the transport of water from the reservoir to the sample could be rate-limiting for the H₂O-uptake of the sample, a dynamic setup was chosen with a small modification compared to the static assembly. Using an adjustable pump, an air stream (0.1–1 ml/s) was blown through the water reservoir or the drying column and then through a small glass tube directly onto the sample.

In experiments at elevated pressures, the water pressure is the same as the total pressure, i.e., the gas phase is composed of essentially pure H₂O. To adjust intermediate pressures (up

Table 2 Summary of water solubility experiments with alkali feldspars

#	Experiment	<i>n</i>	P _{H₂O} (bar)	<i>T</i> (°C)	Time (h)	ppm H ₂ O
SV.M	1 atm, static	2	0.00001	1000	2592	≈ 3
SV.W	1 atm, static	3	0.001	1000	205	26.5 ± 11.1
SV.I	1 atm, static	3	0.006	1000	480	37.5 ± 3.3
SV.V	1 atm, static	3	0.010	1000	139	39.0 ± 0.9
SV.DA	1 atm, dynamic	3	0.010	1000	354	41.1 ± 9.3
SV.DB	1 atm, dynamic	4	0.020	1000	259	59.1 ± 9.6
SV.X	1 atm, dynamic	1	0.025	1000	190	74.7
SV.H	1 atm, static	5	0.035	1000	280	70.2 ± 3.9
SV.DC	1 atm, dynamic	2	0.035	1000	70	54.7 ± 12.9
SV.U	1 atm, static	4	0.035	1000	180	55.0 ± 3.7
SV.Q	1 atm, static	4	0.050	850	1800	87.3 ± 4.5
SV.L	1 atm, static	5	0.050	900	432	89.7 ± 3.4
SV.O	1 atm, static	3	0.050	1000	130	87.6 ± 1.0
SV.DG	1 atm, dynamic	3	0.050	1000	408	96.8 ± 6.1
SV.N	1 atm, static	3	0.050	1050	150	71.4 ± 0.9
SV.P	1 atm, static	3	0.050	1050	204	79.0 ± 5.9
SV.C	1 atm, static	3	0.100	1000	> 343	92.6 ± 5.7
SV.G	1 atm, static	3	0.100	1000	> 93	92.9 ± 2.2
SV.DF	1 atm, dynamic	4	0.200	1000	240	93.9 ± 2.0
SV.S	1 atm, static	6	0.300	1000	162	92.4 ± 1.9
SV.R	1 atm, static	3	0.500	1000	130	103.7 ± 3.5
SV.Y	1 atm, static	3	0.600	1000	250	102.8 ± 5.1
SV.DI	1 atm, dynamic	3	1.000	1000	784	115.9 ± 8.6
SV.QA	Fused silica capsule	4	7.0–3.5	1000	120	107.0 ± 5.4
SV.QC	Fused silica capsule	2	7.3–3.9	1000	95	89.1 ± 3.0
SV.QB	Fused silica capsule	3	16.5–12.6	1000	95	127.1 ± 1.7
SV.HB	CSPV	1	500	800	240	125.6
SV.HC	CSPV	1	500	800	240	112.0
SV.HD	CSPV	1	500	900	240	102.0
SV.HF	CSPV	2	500	900	480	116.9 ± 5.0
SV.HG ^a	CSPV	1	2000	800	96	136.0
S2.A	1 atm, dynamic	1	1.000	1000	282	128.3
A1.A	1 atm, dynamic	1	1.000	1000	282	136.2

^a1M K_{0.95}Na_{0.05}Cl solution

to ca. 15 bar), feldspars were sealed together with Al(OH)₃ powder in evacuated fused silica ampoules. Upon heating, aluminum hydroxide decomposes to Al₂O₃ and H₂O generating a water pressure inside the ampoule. The initial water pressure was estimated by the ideal gas law considering the amount of Al(OH)₃ and the inner volume of the ampoule. Silica glass ampoules can withstand an internal pressure of 20 bar at a temperature of 1000 °C without problems and survive in alkali-poor atmosphere for several days. A disadvantage of this experimental approach is, however, that silica glass tubes are permeable to water at such temperature. Using water diffusion data for silica glass (Behrens 2010), the loss of water during experiment was calculated, and on this basis, the final water pressure was roughly estimated. Consistency of the measured water contents of the feldspars

with data derived by the other techniques gives confidence that this estimation is not too bad.

High-pressure experiments at elevated pressures were performed either in cold seal pressure vessels (CSPV, up to 900 °C) or in an internally heated gas pressure vessel (IHPV, 1000 °C). The samples were sealed in gold capsules (5 mm diameter, 20 mm length) together with ca. 5 wt% H₂O. The crystals were embedded in powder of the same material to minimize stress during compaction at high pressure. The oxygen fugacity was close to that of the Ni/NiO buffer in the CSPV vessel and about 2.6 log units above the Ni/NiO buffer in the IHPV vessel (Schuessler et al. 2008). Variation of oxygen fugacity was not in the focus of this study. Yang (2012) observed for labradorite much higher water solubility at very reducing conditions (Fe/FeO buffer) but in the

f_{O_2} range in which our experiments were performed, Yang (2012) observed only a weak dependence of hydrogen solubility on f_{O_2} .

Alkali exchange experiment

In the case of the sanidine, which contains strongly bound hydrogen defects, it was tested whether hydrogen can be exchanged by alkalis. In a sealed gold capsule (8 mm diameter, 40 mm height), a crystal plate was fixed with a platinum wire at the top of a corundum rod so that the crystal was above a alkali chloride melt (see sketch on right hand side of Fig. 10). Thus, alkalis are provided by the vapor phase, and dissolution reactions of the crystals with the melt are avoided. NaCl/KCl mixtures with intermediate ratio were used to minimize strain and crack formation in the crystals induced by the alkali exchange (Petrishcheva et al. 2018). Under hydrothermal conditions, the exchangeability of hydrogen was tested with a 1 molar $K_{0.95}Na_{0.05}Cl$ solution in a CSPV experiment at 800 °C, 2 kbar.

Results

Water content of starting materials

IR microscopic measurements indicate that H_2O is homogeneously distributed in all the feldspar crystals. The deviation of the local H_2O concentration from the average value was always below 5%. Moreover, polarized spectra show that the pleochroism does not vary within the crystals. This is extremely important because different slabs of each crystal were used in the solubility experiments.

The results of NRA are displayed in Fig. 1. Extremely high hydrogen contents were measured in the first 100 nm near the surface of the crystal plates, probably caused by corrosion during sample preparation and by reaction with atmospheric water. A constant hydrogen level was detected at greater depth which is interpreted as the original water content of the feldspars. Data for (001) and (010) sections of the sanidine S3 agree within analytical error and yield an H_2O content of 194 ± 44 (2σ) ppm. For the plagioclase G2, a slightly lower water content of 130 ± 44 (2σ) ppm was obtained.

Quantification of the water content of feldspars by IR spectroscopy requires measurement of three polarized IR spectra, ideally with the E-vector of the beam oriented parallel to the principal axis of the crystal (Johnson and Rossman 2003). Using the sum of integrated peak intensities of the OH absorption bands, A^* , of these three spectra, the water content C_w , expressed as ppm H_2O by weight, can be determined using the Lambert–Beer law

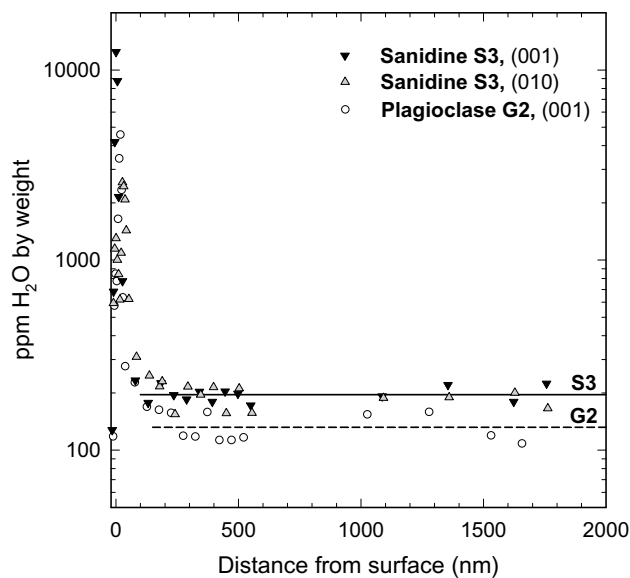


Fig. 1 Results of NRA depth profiling in a sanidine S3 and a plagioclase G2. Horizontal lines represent average water contents in both feldspars. High water contents in the near surface region (< 100 nm) are due to corrosion

$$C_w = \frac{18.02 \cdot A^*}{d \cdot \rho \cdot \epsilon} \times 10^6, \quad (1)$$

where d is the thickness of the section in cm, ρ is the density of the mineral in g/L, and ϵ is the integral molar absorption coefficients in $L \text{ mol}(H_2O)^{-1} \text{ cm}^{-2}$. In anisotropic materials, polarized infrared spectroscopy along any three orthogonal directions can be applied for determination of water contents (Libowitzki and Rossman 1996; Shuai and Yang 2017), which makes sample preparation much easier. This approach was followed in the present study by analyzing spectra perpendicular to (010), perpendicular to (001), and parallel to the crystallographic a axis.

Good agreement with the NRA data was obtained for the plagioclase G2 when using the absorption coefficient of $107,000 \text{ L mol}(H_2O)^{-1} \text{ cm}^{-2}$ which, according to Johnson and Rossman (2003), is applicable to all feldspars with structural hydrogen (Table 1). They used 1H NMR spectroscopy for calibration of the ϵ values. In contrast, with the absorption coefficient of $202,600 \text{ L mol}(H_2O)^{-1} \text{ cm}^{-2}$ derived by Mosenfelder et al. (2015) for type IIa OH using SIMS for calibration, the IR-based C_w values are by a factor of two lower than the NRA analysis. The same applies to the sanidine S3, where the NRA analyses are also larger by a factor of 2 than C_w values obtained by IR spectroscopy using the calibration of Mosenfelder et al. (2015) for type IIb OH ($\epsilon = 150,000 \text{ L mol}(H_2O)^{-1} \text{ cm}^{-2}$). This comparison shows that the absolute determination of the water content of feldspars by IR spectroscopy is still subject to

large uncertainty and depends on the method used for the calibration of the absorption coefficients.

Near-infrared spectroscopy

Combination bands in the NIR can be used to distinguish molecular H_2O (near 5200 cm^{-1}) and OH groups bond to tetrahedral cations (near 4500 cm^{-1}). For oxide glasses and melts with variable water contents, a quantitative determination of species concentrations is possible with the NIR combination bands (Behrens 2020). For feldspars, information on hydrogen defects from NIR spectra is very limited. Single crystals several millimeters in size with high transparency are required due to the low water content. Spectra of the Eifel sanidines and the adularia A1 give clear evidence that OH groups are the dominating hydrogen species, but a small amount of H_2O molecules cannot be excluded as a weak band at 5200 cm^{-1} is also visible (Fig. 2a). The spectrum of the plagioclase G2 shows a broad, poorly resolved peak near 4500 cm^{-1} and no features near 5200 cm^{-1} implying that OH groups in variable environment are present (Fig. 2b). Again, the quality of the spectrum does not exclude a small fraction of H_2O molecules in the plagioclase. In summary, the NIR observations on the feldspars used in this study are consistent with findings on similar materials reported by Johnson and Rossman (2003, 2004).

Mid-infrared spectroscopy

The polarized infrared spectra of the three sanidines used in the present study are basically identical to spectra of Eifel sanidine reported by Beran (1986) and Johnson and Rossman

(2004) (Fig. 3). Two types of OH dipoles are present, one with an absorption maximum at 3400 cm^{-1} (A_{3400}) is aligned parallel to the a axis, the second with an absorption maximum at 3050 cm^{-1} (A_{3050}) is oriented perpendicular to (010), marked as b^* in Fig. 4. The ratio of maximum absorbances, A_{3400}/A_{3050} , seems to depend on the specific crystal but may be affected also by the efficiency of the applied polarizer. For the sanidines used in this study, A_{3400}/A_{3050} of 2.66 ± 0.10 for SV and 2.06 ± 0.10 for S2 were determined. Figures shown by Beran (1986) and Johnson and Rossman (2004) indicate A_{3400}/A_{3050} of 2.2 and 3.4, respectively.

It is striking that the basic pleochroic features are preserved in the sanidine after partial dehydration. In Fig. 4, absorbances at 3400 and 3050 cm^{-1} are compared for virgin and tempered (001) and (010) sections of sanidine SV. Based on the intensity reduction of the 3400 cm^{-1} band, the tempered samples had lost 63% of its initial water content. Both the 3400 cm^{-1} band and the 3050 cm^{-1} band are still present in the (001) section after partial dehydration, indicating that the stability of both defects does not differ much. The A_{3400}/A_{3050} ratio is slightly smaller in the tempered section (≈ 1.3). A similar trend is visible for the (010) section, in which the ratio of maximum absorbance A_{3400}/A_{3050} decreases from 2.6 to 1.7 after partial dehydration. Thus, in both cases, the 3050 cm^{-1} band becomes relatively more pronounced in the partially dehydrated sample. Consistent with the solubility trends in Fig. 11a, this indicates that the natural sanidine contains a small fraction of a second hydrogen defect, probably of type IIa OH, in addition to the predominant type IIb OH defect. However, the change in A_{3400}/A_{3050} may also be due, at least in part, to the baseline correction and the low-peak intensity in the partially dehydrated samples. In

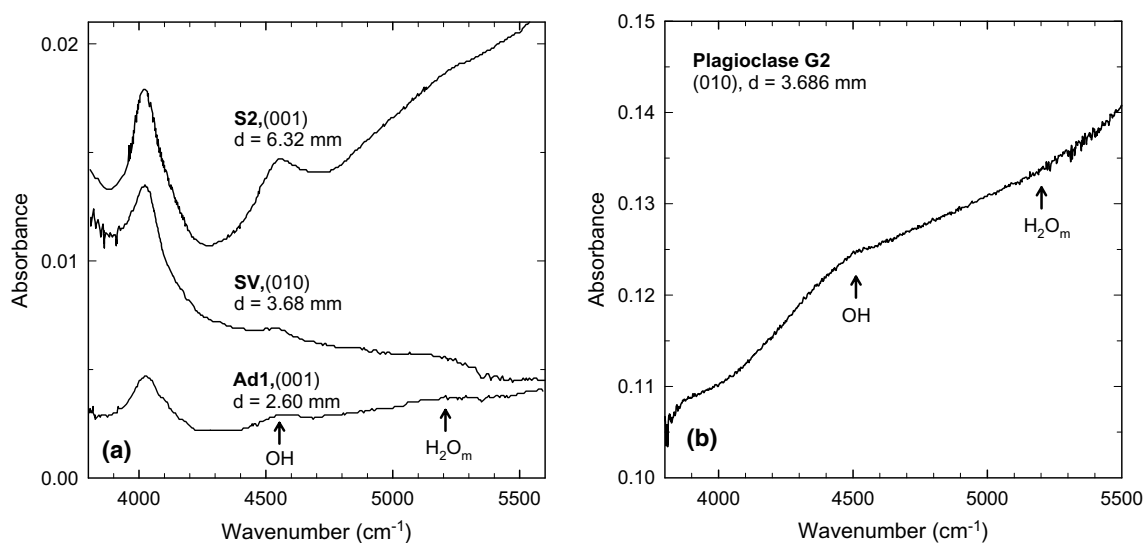


Fig. 2 Near-infrared absorption spectra of three alkali feldspars (a) and a plagioclase (b). The spectra were recorded using a partially polarized beam with the E vector predominantly in the direction of the crystallographic a axis

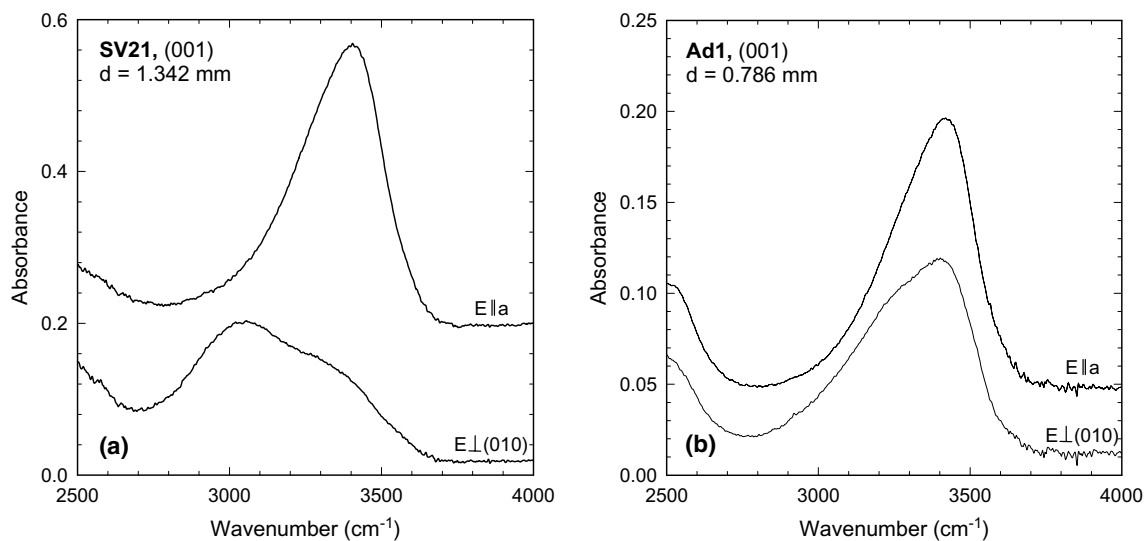


Fig. 3 Polarized IR spectra of (001) sections of a sanidine (**a**) and an adularia (**b**). The two bands at 3050 and 3400 cm^{-1} of the sanidine are characteristic for type IIb OH defects. The dichroic scheme of

the adularia with only one major band at 3400 cm^{-1} represents type IIa OH defects

this study, a linear baseline was chosen as it gives the best reproducibility.

Polarized spectra of the adularia are distinctly different from the sanidine (Fig. 3) in that the band at 3050 cm^{-1} is absent. Thus, the pleochroic scheme of the adularia is more consistent with type IIa OH defects, as observed in volcanic plagioclase (Johnson and Rossman 2003).

The pleochroic scheme of virgin and tempered plagioclase resembles that published in literature (Beran 1987; Johnson 2006), i.e., the dominant OH dipole orientation is roughly parallel to the crystallographic a axis with the maximum absorbance at $\approx 3250 \text{ cm}^{-1}$. Using a polarized beam, for the G2 plagioclase, the ratio of minimum to maximum peak height is 2.23 ± 0.10 on (010) sections and 3.67 ± 0.20 on (001) sections. Comparison with the literature shows that the pleochroism can vary slightly from crystal to crystal. For instance, on (001) section, ratios of minimum to maximum peak height of 3.1 and 3.4 were derived from figures published by Yang (2012) and Beran (1987), respectively. The dichroic scheme was also measured on a 0.737-mm-thick (010) section of G2 which has lost 70% of its initial water content (based on the change in maximum absorbance at 3250 cm^{-1}) after heating at 1000 $^{\circ}\text{C}$. The ratio of minimum to maximum peak height of 2.53 ± 0.25 agrees within error with the virgin sample.

Effect of heating on the OH stretching vibration bands

Heating the sanidine SV for 1 min. to 400 $^{\circ}\text{C}$ gives small but systematic irreversible changes of the OH stretching

vibration bands. The band intensity is slightly reduced at wavenumbers below 3300 cm^{-1} and slightly increased above 3300 cm^{-1} (Fig. 5). In partial polarized spectra of (001) and (010) sections with the electrical field vector predominantly oriented parallel to the crystallographic a axis ($E_{\text{dom}} \parallel a$), the peak height at 3400 cm^{-1} is increased by about 2% and the integrated intensity is reduced by about 1.5% after heating. The spectral features remain unchanged after longer annealing at 400 $^{\circ}\text{C}$ or additional short-term annealing at temperatures up to 800 $^{\circ}\text{C}$. The observed effect of short-term heating at 400 $^{\circ}\text{C}$ is interpreted to be due to a relaxation of the feldspar structure reducing the strength of hydrogen bonding between OH groups and adjacent oxygens. Similar effects by short-term heating were observed for plagioclases.

In Fig. 6, IR spectra measured at elevated temperature (600 $^{\circ}\text{C}$) are compared to room temperature spectra. Generally, the absorbance decreases strongly at low wavenumbers and increases slightly at high wavenumber upon heating. As a consequence, the maximum shifts toward higher wavenumber. At least up to 600 $^{\circ}\text{C}$, the temperature-induced changes are completely reversible, except for the small first-heating effect mentioned before. A key observation for the feldspars used in this study is that the pleochroic features are still present in the high-temperature spectra, i.e., the high- and low-wavenumber component in sanidine, and the preferred OH dipole orientation parallel to the a axis in plagioclase and adularia.

Similar spectral changes upon heating are reported for other feldspars (Liu et al. 2018) and for glasses (Kepler and Bagdassarov 1993; Behrens and Schmidt 1998). Often, these changes have been explained by a decreasing

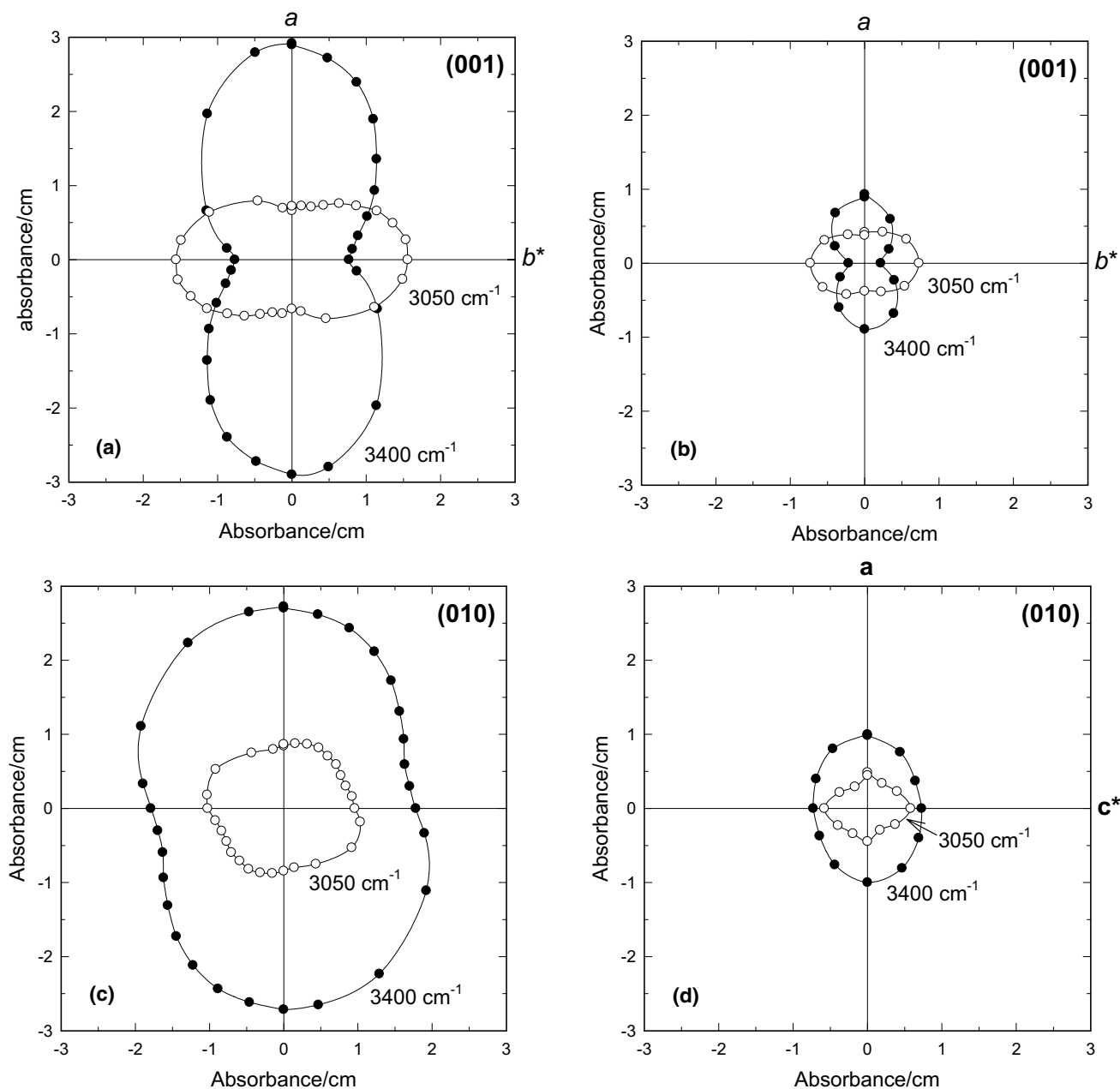


Fig. 4 Dichroic schemes of (001) and (010) sections of sanidine SV before (a, c) and after (b, d) heat treatment for 320 h at 1000 °C, $P_{\text{H}_2\text{O}}=6$ mbar. From the change in A_{3400} , a loss of 63% of the initial

water content is inferred. Basic features are preserved after substantial dehydration, but the band at 3050 cm^{-1} appears to become more pronounced

hydrogen bonding upon heating (Keppler and Bagdassarov 1993; Behrens and Schmidt 1998). In contrary, Liu et al. (2018) interpreted the spectral changes as a re-distribution of hydrogen sites in the feldspar structure which is not quenchable. As outlined by Zarubin (2000), there is little room for such interpretation, and the observed effects can essentially be explained by a temperature-induced

broadening of band components with a simultaneous decrease in intensity.

Annealing of feldspars at controlled $p_{\text{H}_2\text{O}}$

Since the pleochroic scheme of the OH bands is basically preserved after partial dehydration for the volcanic feldspars under investigation, a partially polarized beam with

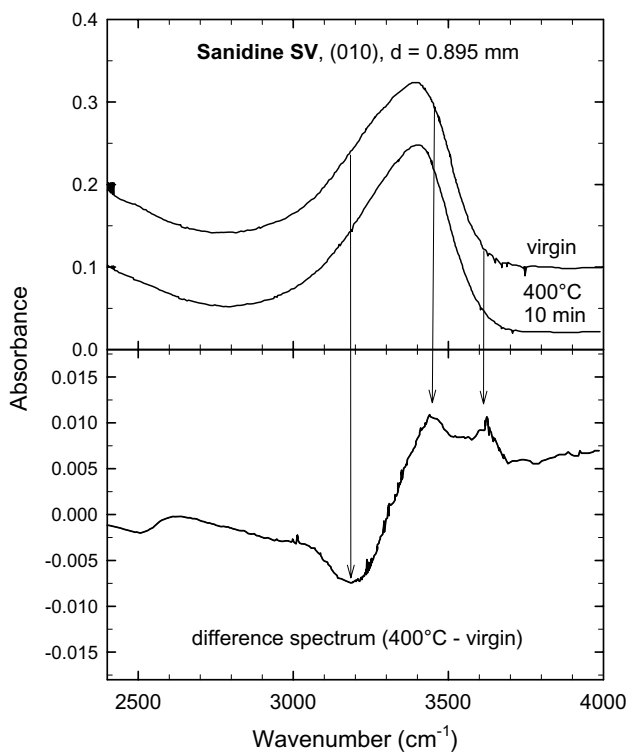


Fig. 5 Effect of short-term annealing on IR spectra of sanidine. Note the different scaling used for the difference spectra on bottom (virgin – 400 °C, 10 min). Arrows mark wavenumbers with pronounced features in the difference spectrum

fixed orientation to the crystal plate was used to track relative changes of the water content after heat treatment. This method has a much better reproducibility than measurements with a polarized beam due to a better signal to noise ratio and a weaker effect of slight misorientation of the crystal to the IR beam. For (010) and (001) sections of the alkali feldspars, the water content was determined by comparing the height of the 3400 cm^{-1} band with the initial height ($A_{3400}/A_{3400,\text{initial}}$). In the case of the plagioclases, the maximum absorbance at 3250 cm^{-1} was compared to the initial value of plagioclase G2 ($A_{3250}/A_{3250,\text{G2, initial}}$) scaled to same thickness (Table 3).

Absolute water contents were calculated by multiplying the ratios with the water content of the respective crystal given in Table 1. For internal consistency and comparison to data published in the literature, the IR calibration of Johnson and Rossman (2003) was used. If in the future, a generally accepted calibration of the OH absorption bands of feldspars should be available, the data can be easily converted. Results of the long-term experiments are summarized in Table 2 and 3, details are given in the supplement Tables S1 and S2.

The behavior of sanidine crystals during heating at 1000 °C , 1 atm under extremely dry conditions is illustrated in Fig. 7a. Two samples [M4(010) and M5(001)] with

about 1.3 mm thickness were used to study the kinetics of water release. After a rapid initial water loss, the kinetics of dehydration considerably slow down and both samples still contain 25% of the initial water content after 432 h. Two thinner samples [M3(010) and M1(001)] were applied to test whether complete removal of H_2O can be achieved at such dry conditions. After 792 h, about 98% of H_2O was lost from both sections. But even after heating for 108 days at 1000 °C , a small OH peak was visible in the IR spectra of these samples, corresponding to a water content of $\approx 3\text{ ppm}$.

All four samples contained numerous cracks after the experimental series, indicating stresses in the crystals imposed by the dehydration reaction. A $3 \times 3 \times 5\text{ mm}$ cuboid was held at same conditions for 18 days, and a section was cut perpendicular to the central axis in the middle of the sample. IR microscopic measurements of the polished section show that 45% of the initial water content was lost, but no diffusion profile was detected although millimeter-sized areas without cracks were present (Fig. 8). This observation implies that either water release is not controlled by diffusion or diffusivity decreases strongly with decreasing water content.

After dehydration in P_2O_5 -dried atmosphere at 1000 °C , the samples M4(001) and M5(010) were used together with a fresh sample in a subsequent experiment at a water pressure of 100 mbar (Fig. 7b). The same final water content (75% of $C_{\text{w, initial}}$) was reached in all samples, indicating that equilibrium of the sample with the applied water pressure was reached. The kinetics of equilibration was much faster in the water-rich sample than in the partially dehydrated samples, i.e., within 75 h, the virgin sample has reached a constant water content while the pre-dried ones need more than 400 h.

A 1-mm-thick (001) section of plagioclase G2 is completely free of water after 200 h at 1000 °C , $p_{\text{H}_2\text{O}} = 1\text{ mbar}$, i.e., in a much shorter time than the sanidine despite of larger sample thickness (Fig. 7c). This implies that dehydration kinetics is much more sluggish in the sanidine, at least in the final stage of dehydration. At 1000 °C , $p_{\text{H}_2\text{O}} = 1\text{ bar}$ three different plagioclases with different initial water content were run simultaneously (Fig. 7d). Within 45 h, a constant water content was achieved in all three samples, but at different levels. Final water content varied from 52 ppm (G2) over 39 ppm (P8) to 20 ppm (P6). The experiment gives evidence that in volcanic plagioclase even at relatively low water pressure a considerable amount of H_2O can be stored. However, it is worth noting that in a long experiment with duration of 900 h, the water content was drastically lowered, i.e., to 20 ppm in G2, 14 ppm in P6 and 12 ppm in P8. This observation indicates that the hydrogen hosting defects in the feldspar structure are not stable under these conditions for very long time.

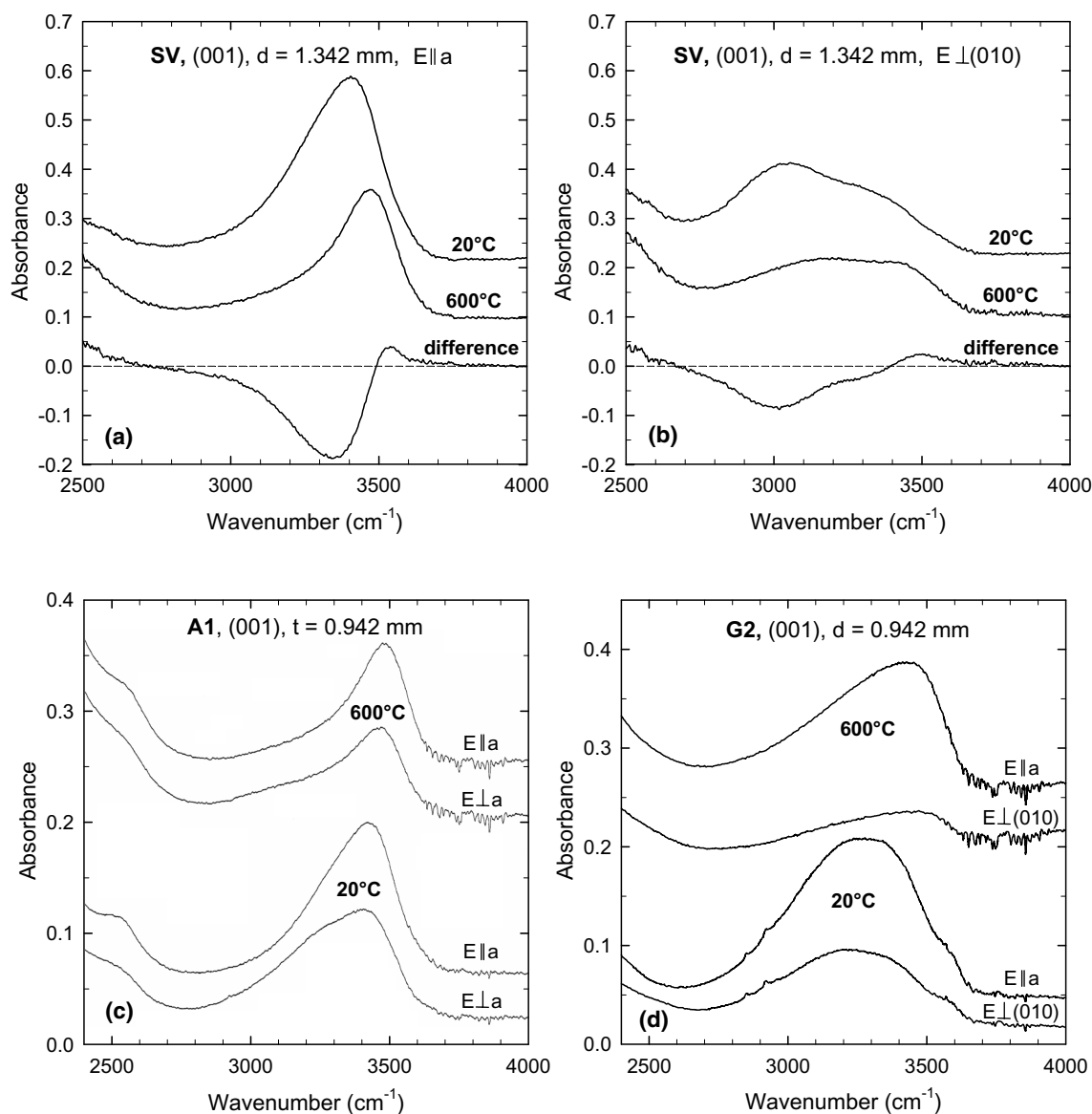


Fig. 6 IR spectra of feldspars recorded on a heating stage with a polarized beam at 20 °C and 600 °C. **a, b** Spectra of sanidine SV with the E vector parallel to the principal OH dipole orientations parallel to the *a* axis (maximum at 3400 cm^{-1}) and perpendicular to (010)

(maximum at 3050 cm^{-1}). Temperature-induced changes are highlighted by the difference spectra on bottom. **c** Spectra of the adularia A1. **d** Spectra of the plagioclase G2

In a second experiment at 1000 °C, $p_{\text{H}_2\text{O}} = 1$ bar a similarly drastic decrease of the water content was observed after 800 h (P6.PB in Table S2a in the supplement). A question is whether this effect is related to change in defect chemistry of the plagioclase induced by oxidation of ferrous iron (Behrens et al. 1990). Experiments with plagioclases pre-annealed for 15 days at 1220 °C in air give no clear answer. In two cases, the water content in the pre-annealed samples was significantly lower than in virgin samples (P6.PB in the supplement table S2a; and P6.QB in the supplement table S2b). In other cases, i.e., P6.IE (see supplement Table S2b), the sample pre-annealed in air did not show

anomalously low water contents. Thus, the mechanism of long-term degradation of defects in plagioclase remains unclear.

An example of high-pressure experiments with plagioclase is given in Fig. 7e. Two partially dehydrated (001) sections of G2 were run in the same capsule at 900 °C, $p_{\text{H}_2\text{O}} = 500$ bar. After 544 h, the water content of both sections was about 20% higher as that of the virgin G2 plagioclase. The data of P6 obtained under same conditions but in separate experiments show the same trend. After 816 h, considerable surface alteration of the P6 sample was visible, resulting in poor IR transmission. After polishing away

Table 3 Summary of water solubility experiments with plagioclase

#	Sample	<i>n</i>	Experiment	P _{H₂O} (bar)	<i>T</i> (°C)	Time (h)	ppm H ₂ O
G2.PC1	G2	1	1 atm, static	0.001	1000	200	5.0
G2.PC3	G2	1	1 atm, static	0.01	1000	200	17.2
G2.PB	G2	1	1 atm, static	0.1	1000	290	15.8
G2.PA	G2	1	1 atm, dynamic	1	1000	135	53.4
						900	20.3 ^a
G2.QA	G2	2	Fused silica capsule	12.6–7.7	1000	118	59 ± 18
G2.QB	G2	4	Fused silica capsule	13.5–10.4	1000	70	98 ± 31
G2.IC	G2	3	IHPV	100	1000	120	123.0 ± 7.2
G2.IA	G2	3 × 2	IHPV	500	1000	140–320	127.5 ± 4.2
G2.HB	G2	2	CSPV	500	900	544	115.1 ± 9.0
G2.IE	G2	2	IHPV	2000	1000	110	165 ± 28
P6.PB	P6	1	1 atm, static	0.1	1000	290	9.8
P6.PA	P6	1	1 atm, dynamic	1	1000	135	20.7
						900	14.3 ^a
P6.PB	P6	2 × 2	1 atm, dynamic	1	1000	139–230	21.1 ± 6.7
P6.QA	P6	2	Fused silica capsule	12.6–7.7	1000	118	60 ± 32
P6.QB	P6	4	Fused silica capsule	13.5–10.4	1000	70	91 ± 28
P6.IC	P6	2	IHPV	100	1000	216	94.9 ± 3.0
P6.IA	P6	2	IHPV	500	1000	60–240	132.7 ± 3.0
P6.Hy06,10	P6	2 × 2	CSPV	500	800	240	168 ± 18
P6.Hy01,07,09	P6	3	CSPV	500	900	240–288	146 ± 21
P6.IE	P6		IHPV	2000	1000	110	241 ± 31
P6.Hy09	P6	1	CSPV	5000	800	240	217.0
P8.A	P8	1	1 atm, dynamic	1	1000	135	37.2
						900	12.4 ^a

Water contents refer to the IR calibration of Johnson and Rossman (2003). Errors represent one standard deviation if more than one sample (*n*) was used in the experiment. Details are given in the electronic supplement

^aDramatic decrease in water content after long-term annealing indicates an irreversible destruction of defects

50 μm on each side, a clear core section remained. Absorbance/thickness ratios of the unpolished and the polished section do not differ significantly (Table S2b in the supplement). The increasing water content up to 816 h implies that equilibrium was not reached in the sample. This contrasts with the study of Yang (2012), who suggest equilibrium of 1 × 1 × 1.5 mm blocks of labradorite with an H₂O fluid within 100 h at a pressure of 2 kbar and temperatures of 800–850 °C.

Alkali-exchange experiment

A sanidine section pre-equilibrated at 1000 °C, 1 atm with a water pressure of 100 mbar lost nearly the whole structural hydrogen within 24 h in a vapor of (Na,K)Cl (Fig. 9). On the one hand, this indicates that the water pressure in the capsule is very low due to H₂O sorption in the molten salt. On the other hand, it shows that hydrogen incorporated in the sanidine structure can be easily substituted by alkali cations. This supports the idea that hydrogen is incorporated as

a proton, which serves as a charge balance, e.g., for excess aluminum on a tetrahedral site. Surprisingly, the hydrogen defect was re-formed by tempering at 300 mbar water pressure to the same extent as before. Even at lower water pressure, at least a partial recovery of hydrogen defects in (Na,K)Cl pre-treated sanidines was observed at 1000 °C (Table S1a in the supplement). For example, at p_{H₂O} = 6 mbar, the water content increased within 205 h to 30% of initial water content of the sanidine.

Such strong recovery is not expected if hydrogen occupies a regular alkali site in the feldspar structure. Heating experiments performed by Behrens and Müller (1995) have shown that hydrogen feldspar (HAlSi₃O₈), produced by an exchange of alkali by protons in sulfuric acid at 280 °C, is thermodynamically instable and decomposes upon heating above 500 °C. In contrast to Na⁺ and K⁺, protons are only bound to a single oxygen and cannot balance the excess charge on the four O atoms around one Al atom in the network structure of the feldspars. It is therefore highly probable that the

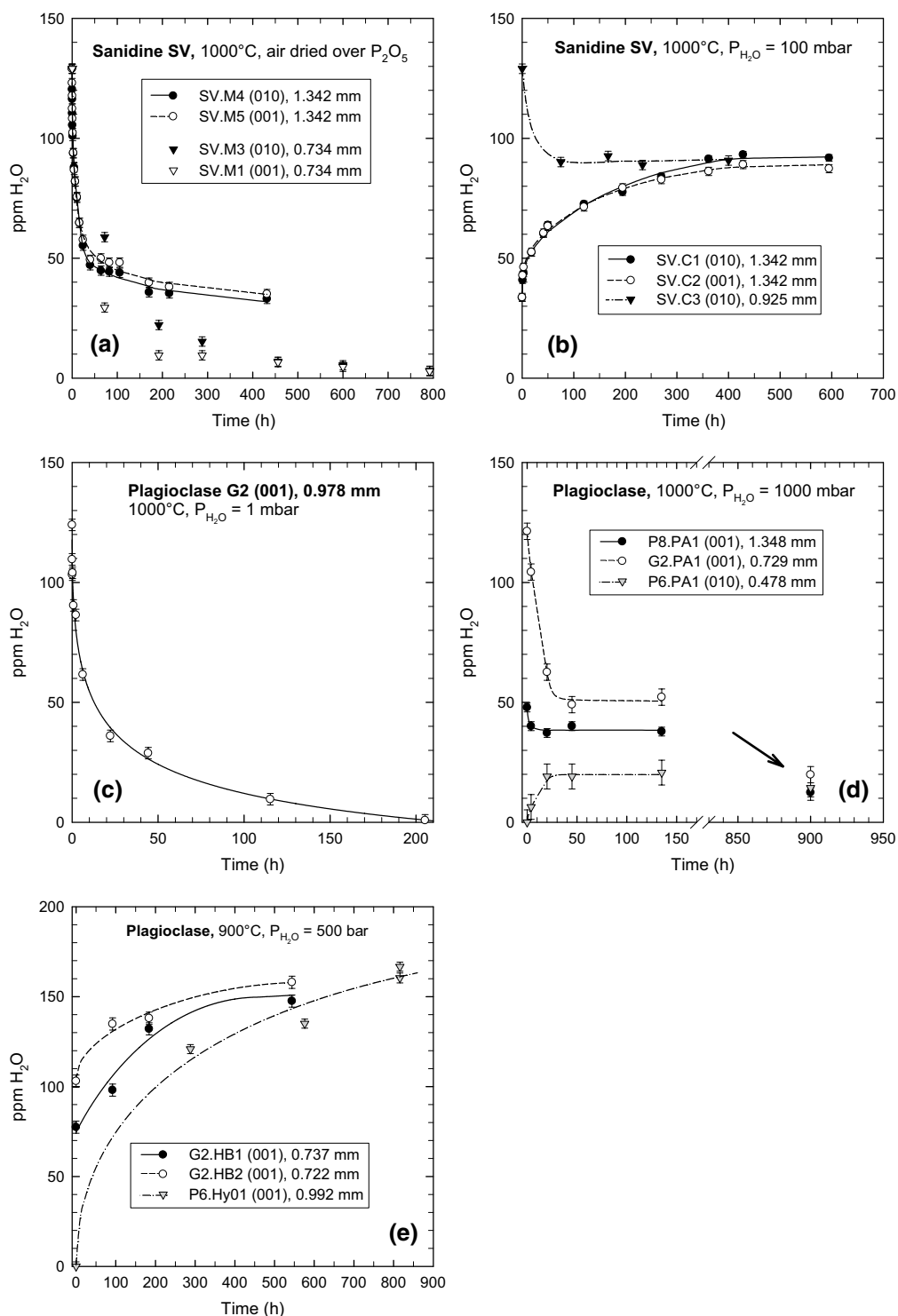


Fig. 7 Development of water contents of feldspar sections during heating at controlled water pressure. **a** Dehydration of sanidine in air pre-dried with phosphorus pentoxide at 1000 °C. The initial period was used to estimate the diffusion coefficient for the mobile water species. Note that the mobility of water species is strongly decreased at high degrees of dehydration. **b** Equilibration of sanidines with different initial water content at a water pressure of 100 mbar and a temperature of 1000 °C. Samples C1 and C2 are the products of M4 and M5, respectively, from the experiment shown in **a**. Note that equilibrium is reached much faster in the

highly dehydrated samples. **c** Dehydration of a plagioclase section at 1000 °C at relatively low water pressure. Fitting of the initial period was used to estimate the diffusivity for water-rich plagioclase. Note the release of water considerably slows down at low water contents. **d** Equilibration experiment with three plagioclases at a water pressure of 1 bar at 1000 °C. **e** Experiments with plagioclase sections under hydrothermal conditions at 900 °C, 500 bar. The trials were interrupted to record IR spectra and then the samples were welded into new gold capsules together with H₂O for the next heating period

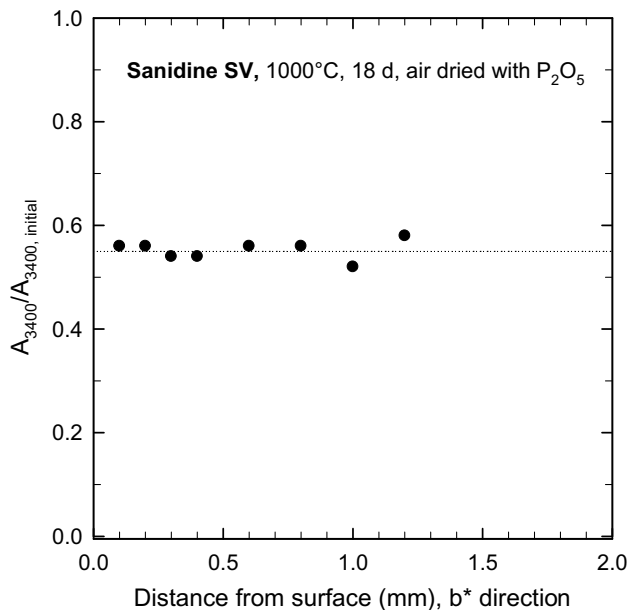
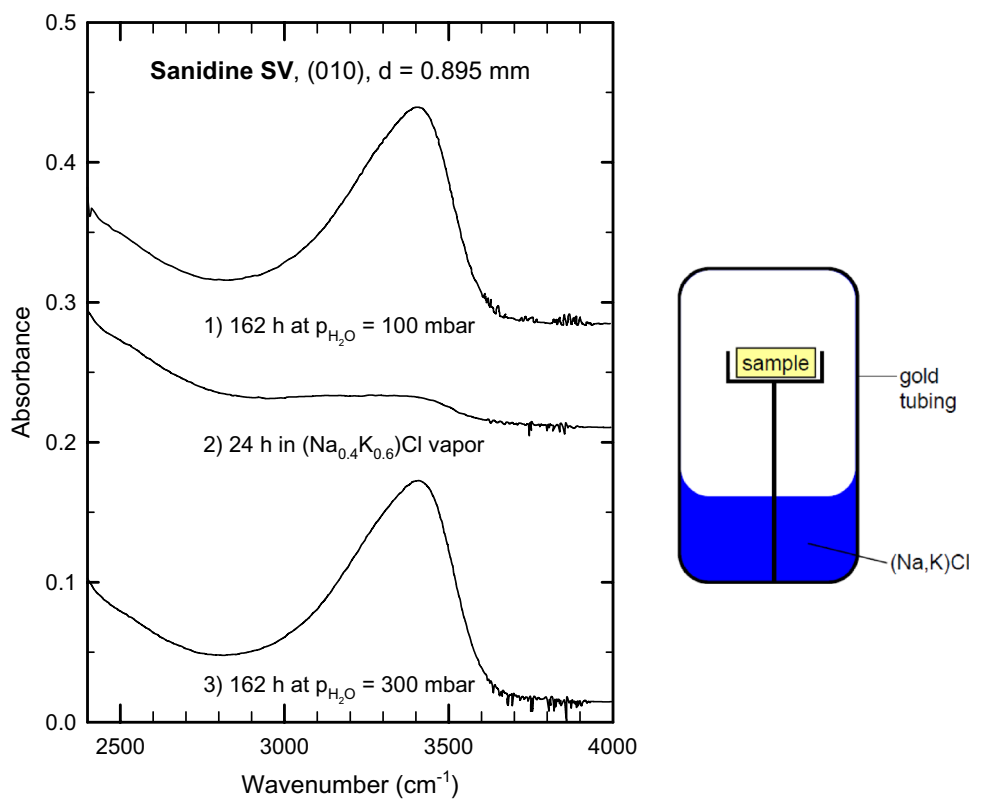


Fig. 8 OH profile in a sanidine cuboid (3×3×5 mm) after a dehydration experiment at extremely low water pressure

Fig. 9 Development of the IR spectrum of a sanidine section during heat treatment at different conditions. (1) after 250 h at 1000 °C, $P_{H_2O} = 100$ mbar the water content is reduced by 25%. (2) Within 24 h at 1000 °C in (Na,K)Cl vapor, adjusted using the setup on right, the water content dropped to 2%. (3) Subsequent heating for 162 h at 1000 °C, $P_{H_2O} = 300$ mbar produced the same water content as present before the alkali chloride treatment



protons are located on an interstitial site and not on a regular alkali site.

Hydrothermal experiments with sanidine sections and alkali chloride solutions at 800 °C, 2 kbar gives no indication

for an exchange of protons by alkalis. Water contents measured by IR after 24 h and 96 h are about the same as that of the starting sanidine SV (Table S1b in the supplement). This confirms that alkalis can replace hydrogen only in absence of H₂O in the surrounding atmosphere.

Discussion

Diffusion of hydrogen species in feldspars

Although diffusion is not the main target of this paper, some conclusion can be drawn from the dehydration experiments. In most cases, polished plates were used where the width was many times greater than the thickness. Thus, boundary condition was an infinite plane sheet with an initial uniform distribution of hydrogen. Assuming that the diffusion coefficient D is constant, and water can be released completely, the dehydration of a sheet with thickness d can be described by the respective solution of Fick's 2nd law (Crank 1975)

$$\frac{M(t)}{M_\infty} = 1 - \frac{8}{\pi^2} \sum_{n=0}^{\infty} \frac{1}{(2n+1)^2} \cdot \exp\left(- (2n+1)^2 \cdot \frac{\pi^2}{d^2} \cdot Dt\right), \tag{2}$$

in which $M(t)$ is the fraction of diffusing substance that has left the sheet after time t and M_∞ is the amount of diffusing

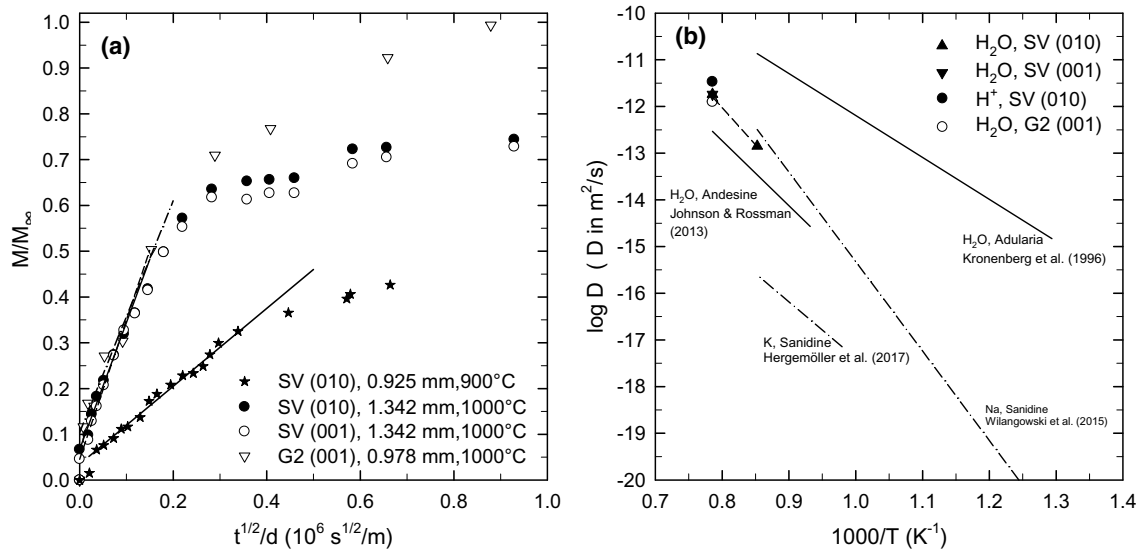


Fig. 10 **a** Plot for determination of the diffusion coefficients for dehydration experiments with sanidine SV and plagioclase G2. Lines are regressions of the data at low degrees of dehydration. Solid lines: SV (010); dashed line: SV (001); dash-dotted line: G2 (001). **b** Selected diffusion data for feldspars. Solid lines refer to dehydration experiments of Kronenberg et al. (1996) and Johnson and Rossman (2013).

substance that has left the sheet after infinite time. In the initial stage of dehydration, the fractional loss of hydrogen is proportional to the square root of time:

$$\frac{M(t)}{M_{\infty}} = \left(\frac{16 \cdot D}{\pi} \right)^{0.5} \cdot \frac{t^{0.5}}{d}. \quad (3)$$

This simplified equation applies for $M(t)/M_{\infty} < 0.5$, i.e., till the profiles from both sides of the sheet start to overlap significantly. The four experiments in which spectra were initially recorded at short intervals are presented in Fig. 10a. After initial disturbances, which are probably related to the individual heating/cooling increments during stepwise heating, a linear dependence of $M(t)/M_{\infty}$ on $t^{1/2}$ was observed for all samples. In the case of the plagioclase, this relationship applies up to 50% water loss. Also, the relatively fast complete dehydration of the plagioclase indicates that the above-mentioned conditions are fulfilled. In contrast, the sanidines show a noticeable negative deviation from the expected trend already from 30% water loss. Such a deviation may be explained by a strong concentration dependence of water diffusivity. However, it should be noted that such time-dependent bulk measurements with plane sheets are not suitable for determining a concentration dependence of diffusion coefficients. A weak dependence is not even discernible from these measurements and would be consistent with the data for the plagioclase.

Water diffusion coefficients derived by Eq. (3) are compared to other diffusion data based on dehydration

Self-diffusivities of Na and K in sanidine from Wilangowski et al. (2015) and Hergemöller et al. (2017) are shown as dash-dotted lines for comparison. Size of symbols used for the data of the present study correspond to their error. The dashed line is a regression to the data for initial dehydration of sanidine

experiments with feldspars in Fig. 10b. At 1000 °C, diffusion coefficients for two different orientations of the sanidine agree within error, indicating an isotropic diffusion behavior, consistent with findings for andesine by Johnson and Rossman (2013). These $D_{\text{H}_2\text{O}}$ values, representing the initial stage of dehydration of sanidine, are in good agreement with the measured value for the plagioclase G2. This may indicate that a fraction of hydrogen is bound in type IIa OH defects, similar as in plagioclase. But one needs to be aware that the diffusion coefficients for the sanidines are only rough approximations, since the boundary conditions for Eq. (2) are not fully satisfied. The dehydration experiment with sanidine SV at 900 °C can be used to estimate the temperature dependence of water diffusivity in sanidine, although the data set is too poor for a proper determination of the Arrhenius law. The preliminary equation is $D_{\text{H}_2\text{O}}(\text{m}^2/\text{s}) = 5.2 \exp(-36,600/T)$ where T is inserted in K.

The $D_{\text{H}_2\text{O}}$ values are higher by 0.5 log units than data derived from dehydration of andesine (Johnson and Rossman 2013). The experimental data of Johnson and Rossman (2013) were reproduced by Zhang et al. (2016) through a thermodynamic model that interconnects point defect parameters with bulk properties. A reason for the deviation of my data to those of Johnson and Rossman (2013) could be the higher water content of the andesine of 510 ± 90 ppm compared to the labradorite G2 (124 ± 15 ppm). If the concentration of mobile hydrogen species is the same in both minerals at given p , T conditions, the difference in diffusivity may simply reflect the different ratio of stationary defects to

mobile defects. Such an approach can also explain the much higher diffusivities measured by Kronenberg et al. (1996) on an adularia with thermal instable hydrogen defects. The temporary binding of the water molecules to stable defects in the feldspar structure reduces their mobility in andesine and labradorite. Such a binding does not occur in the case of the adularia of Kronenberg et al. (1996).

The alkali exchange experiment in Fig. 9 can be used for a rough estimate of the corresponding diffusion coefficient. After 24 h, M/M_∞ in a plate of 0.895 mm was about 0.03. The diffusion coefficient calculated by Eq. 2 is $D_H = (3.3 \pm 0.8) \cdot 10^{-12} \text{ m}^2/\text{s}$, where the error results mainly from the uncertainty of the determination of the final water content. The D_H value at such anhydrous conditions most likely represents the interdiffusion of protons with cations. Self-diffusion in sanidine from Volkesfeld is faster for Na^+ ($D_{\text{Na}} = 8.77 \times 10^{-13} \text{ m}^2/\text{s}$, extrapolated to 1000 °C; Wilangowski et al. 2015) than for K^+ ($D_{\text{K}} = 1.58 \cdot 10^{-15} \text{ m}^2/\text{s}$ extrapolated to 1000 °C; Hergemöller et al. 2017). Thus, most likely, the release of hydrogen is controlled by H/Na interdiffusion in these experiments.

D_H is higher by a factor of 4 than D_{Na} but D_{Na} is not rate-limiting since the concentration of Na is much higher ($\text{Na}/\text{H} = 39$ in the virgin sanidine SV). Because of charge neutrality, the exchange reaction requires identical counter fluxes of alkali and protons. Assuming that only Na^+ contributes to the exchange, the condition $c_{\text{Na}} D_{\text{Na}} = c_{\text{H}} D_{\text{H}}$ must be fulfilled. It is striking that removal of hydrogen can occur by a similar speed either by proton diffusion or by water diffusion, depending on the prevailing conditions. However, more data are required to confirm this finding.

Solubility of H_2O in feldspar

Water contents in alkali feldspars and plagioclases after long-term heating at controlled water pressure are displayed in Fig. 11. Data for sanidine at ambient total pressure are bracketed using starting samples with high and low water content and can be interpreted as representing water solubility (Table S1a). At higher total pressure, it is not approved that the duration was sufficient to establish equilibrium conditions, and the measured water content of the sanidines represent minimum values of water solubility (Table S1b).

For plagioclase at 1 atm, the uptake of water by the initially anhydrous P6 and the water loss of the hydrous G2 in the same experiment can be considered as a bracketing of water solubility as well (Table S2a). However, the concentration of extrinsic defects which can host H_2O may be different in both crystals. The water solubility in the plagioclases at intermediate pressure is better constrained at least for experiment QA (Table S2b), since bracketing is evident both for G2 and P6 (a hydrothermally pretreated P6 sample was included in the sample set). The average water

content of all four samples after heat treatment for 118 h was $(60 \pm 21) \text{ ppm H}_2\text{O}$. However, the water pressure could be only roughly estimated for this experiment (7.7–12.6 bar). In the second run, QB with plagioclases in a silica ampoule for 70 h at 1000 °C, the water content of all loaded plagioclases increased, and the final values represent minimum water solubilities. Bracketing of water solubility could be also achieved for plagioclase G2 at 1000 °C; $p_{\text{H}_2\text{O}} = 100 \text{ bar}$ with $(123 \pm 7) \text{ ppm H}_2\text{O}$. All other experiments with plagioclase at high pressure yield an increase of the water content and, hence, only minimum values of the water solubility.

It is striking that in all igneous feldspars, a noticeable amount of water could be dissolved already at a geologically low water pressure of 1 bar. For the three plagioclases, the water content under these conditions ranged between 20 and 37 ppm (Fig. 11b). The water content of the alkali feldspars was even higher, between 114 and 146 ppm (Fig. 11a). At pressures between 50 and 300 mbar, the water content of sanidine SV was constant at approx. 75% of the initial content. At lower $p_{\text{H}_2\text{O}}$, a strong decrease of the water content can be observed. However, the scattering of the data indicates that, due to kinetic problems, an equilibrium may not yet have been reached. Above a partial water pressure of 300 mbar, the water content of the sanidine increases again. The experiments in the silica ampoules are in line with the trend, but show a noticeable scattering of the data, which can be attributed to an inaccurately determined and time-variable water pressures. Higher pressures were not tested with the sanidine at 1000 °C because the formation of even small amounts of water-rich melts inside the crystal could falsify the results. Long-term experiments in an CSPV at 800–900 °C and 500 bar water pressure yield water contents of the sanidine SV slightly lower than the initial water content (between 102 and 126 ppm H_2O).

Plagioclases show a systematic increase of the water content with increasing $p_{\text{H}_2\text{O}}$ above 0.1 bar (Fig. 11b). Maximum values were found in the initially water-free plagioclase P6 with 219–263 ppm H_2O at 1000 °C; 2 kbar and 217 ppm at 800 °C, 5 kbar (see Table S2b in the supplement). The water contents of the labradorites at high pressures in my study are noticeably higher than reported by Yang (2012) for a similar material. He concluded that equilibrium was attained from experiments with different duration and from the absence of noticeable variation of the OH absorption bands from rim to core. However, variation in run duration was relatively small in his experiments (e.g., 100 h and 155 h at 800 °C, 2 kbar, NNO buffer) and, as illustrated in Fig. 8, the absence of a diffusion profile is not a clear proof for the establishment of equilibrium. Considering the diffusion data for plagioclase in Fig. 11b, it is surprising that the experimental time should have been sufficient to homogenize water distribution in a plagioclase with minimum dimensions of 1 mm, as used by Yang (2012).

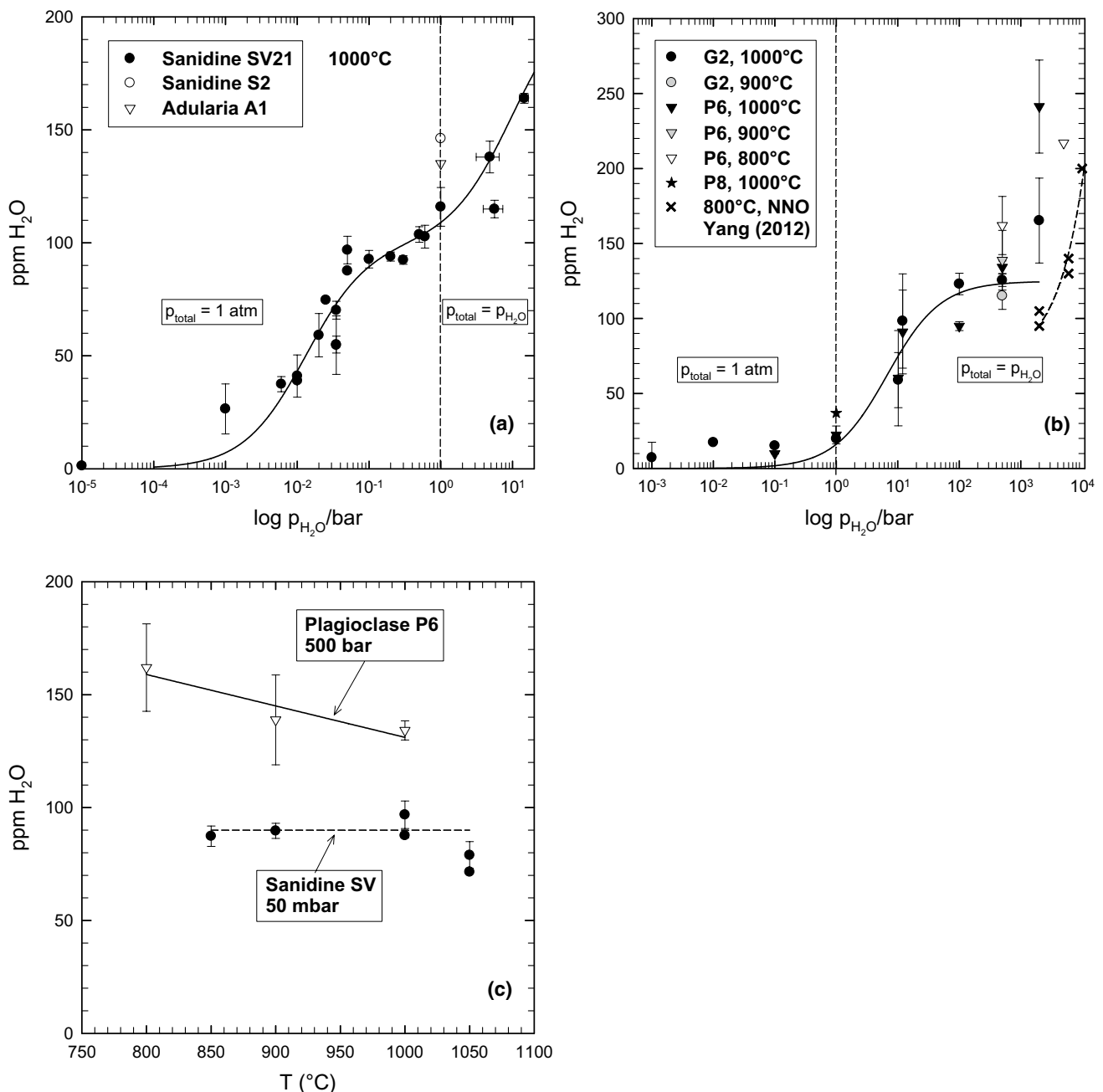


Fig. 11 Results of long-term annealing of volcanic feldspars at constant water pressure. See text for detailed discussion. **a** Effect of water pressure for alkali feldspars at 1000 °C. The vertical dashed line separates the region with constant pressure from that with $p_{\text{total}}=p_{\text{H}_2\text{O}}$. The solid line is a fit of data of sanidine SV assuming two different hydrogen defects. **b** Effect of water pressure for plagioclase. The vertical dashed line separates the region with constant pressure from that

with $p_{\text{total}}=p_{\text{H}_2\text{O}}$. The solid line is a fit of the data of the three plagioclases by a Langmuir model up to 500 bar. Results of solubility experiments of Yang (2012) are shown for comparison. **c** Variation of temperature for sanidine and plagioclase at selected water pressure. The decrease of water content of sanidine at 1050 °C is attributed to an instability of type IIb OH defects at high-temperature/low water pressure

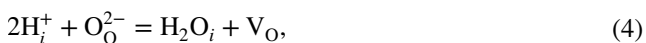
The temperature effect on water solubility was not systematically studied. Data for the plagioclase P6 indicate a slight decrease of water content with increasing temperature at 500 bar water pressure (Fig. 11c). This trend is not consistent with the findings of Yang (2012) who reported

an increase of water solubility with temperature for a pressure of 2 kbar. For the sanidine SV at $p_{\text{H}_2\text{O}}=50$ mbar, no variation was found between 850 and 1000 °C, but a small decrease toward higher temperature. However, as noted before, kinetics play a major role for adjustment of the low

water content in the sanidines and, thus, the lower values at 1050 °C may be due to faster kinetics at higher temperature.

Hydrogen defects

The spectroscopic and experimental findings strongly indicate that water solubility in igneous feldspars is strongly affected by other defects which were either incorporated during crystal growth or have been formed later on by intracrystalline diffusion. The sanidine contains at least two different defect types with differently strong local binding of the hydrogen and, hence, different mobility of hydrogen. The type IIb OH defect (Johnson and Rossman 2003) is most likely a substitution of Si^{4+} by Al^{3+} and H^+ (AIOH defect). Such substitution is very common in quartz (Kats 1962; Aines et al. 1984). AIOH defects in quartz have a very high-temperature stability, persisting to over 1200 °C at 1 atm (Kats 1962). These centers in quartz can be destroyed by intense electrolysis in a vacuum, resulting in oxygen vacancies forming the charge compensation for Al^{3+} . The behavior of the strongly bonded H defects in sanidine is rather similar. The H defect is stable under relatively dry conditions ($p_{\text{H}_2\text{O}} \ll 1$ bar) at 1000 °C and cracks are formed during dehydration which can be explained by strain of the network upon formation of oxygen vacancies V via



where i refers to interstitial sites and O to oxygen sites. The assignment of H^+ to interstitial sites is supported by the alkali exchange experiments, i.e., by the complete reformation of this defect when some water vapor is present. A direct proof of such substitution scheme based on composition is not possible since Al is a major component in feldspars. Using the water content of sanidine S3 by NRA and assuming that 75% of hydrogen is bond in AIOH defects, the ratio of $\text{Al}_{\text{total}}/\text{AIOH}$ is 230:1. Considering that the accuracy of electron microprobe for Al_2O_3 is about 1%, there is no chance to detect such small excess of Al compared to the ideal feldspar composition.

The second H-bearing defect in sanidine, stable at elevated water pressures, is probably a type IIa OH defect as found in plagioclase and the adularia A1. The easy mobilization of H_2O from such defect can be explained by a neutral associate of H_2O molecules with a pre-existing defect in the feldspar structure. Such a defect can be, for instance, a vacancy on the site usually occupied by an alkali cation (A1 site). Formation of such kind of defect by incorporation of excess of silica as a $\text{V}_{\text{Al}}\text{Si}_4\text{O}_8$ component has been suggested by Behrens et al. (1990) based on oxidation-induced changes in sodium diffusivity. For plagioclases as used in the present study, Behrens et al.

(1990) suggested that 0.29% to 0.36% of the A1 sites are empty. This corresponds to an excess of silica of ≈ 0.1 wt%. Thus, as for the postulated AIOH defect in sanidine, it is not possible to detect such deviation from stoichiometric feldspar composition by currently available analytical techniques. The association reaction can be described as



where the brackets indicate an associate. For minimization of local energy, the associate may react with network oxygen producing 2 OH groups, as indicated by NIR spectroscopy



The V_{Al} contents estimated by Behrens et al. (1990) for three plagioclases correspond to maximum water contents of 190–240 ppm, if reaction (5) controls the incorporation of water in the feldspar. The measured water contents in this study are consistent with such an incorporation mechanism, however, no saturation of the defects can be seen in the tested pressure range.

As outlined before, under hydrothermal conditions, the mobile species in feldspars are most likely H_2O molecules on interstitial sites. This thesis is particularly supported by oxygen diffusion data (Yund and Anderson 1974; Giletti et al. 1978; Elphick et al. 1988; Farver and Yund 1990; Farver 2010) which can be best explained by diffusion of an O-bearing carrier molecule (Doremus 1998). Protons only play a role as mobile species in a dry, alkali-rich environment, but this situation is hardly relevant geologically. At the crystal surface, the concentration of H_2O_i is determined by the prevailing water vapor through the reaction



where g signifies a vapor phase. In the crystal interior, the defect reactions (Eq. 4) and (Eq. 5) control the local concentration of H_2O_i . The higher the degree of dehydration, the greater the concentration of V_O (Eq. 4) or V_{Al} (Eq. 5) and, thus, the greater the probability of H_2O_i trapping. Therefore, a particularly strong negative correlation of $D_{\text{H}_2\text{O}}$ to c_w is expected if the binding energy between existing defect and H_2O_i is large. This is the case for the postulated AIOH defect.

Modeling of water solubility in feldspars

In a simple modeling of the water solubility data, it is assumed that the interaction energy of H_2O_i and vacancies depends only on the type of the vacancy (V_O or V_{Al}) but not on their concentration. The concentration of the vacancies is a specific constant for each crystal. Such behavior can be described by a Langmuir isotherm

$$c_w = \frac{c_{w,0} \cdot K \cdot p_{H_2O}}{1 + K \cdot p_{H_2O}}, \quad (8)$$

where $c_{w,0}$ is the maximum amount of H_2O that can be bound in the defect and K is the Langmuir constant which characterizes the binding energy between the H_2O molecule and the defect center. The solid line in Fig. 9b shows the fit to all plagioclase data at 1000 °C. In fitting, K and $C_{w,0}$ have been adjustable parameters. Assuming that $C_{w,0}$ does not differ for the three plagioclases used in the study, the values obtained are $C_{w,0} = (124.8 \pm 7.8)$ ppm H_2O and $K = (0.148 \pm 0.42)$ ppm⁻¹ bar⁻¹ with a correlation coefficient $r^2 = 0.92$. The general trend of the data is well described, but a higher $C_{w,0}$ is expected when considering the high-pressure solubilities at lower temperature and the estimated concentration of A1 vacancies.

The data of sanidine at 1000 °C could be modeled very well by a combination of two Langmuir isotherms (Fig. 9a). First, an isotherm was fitted to the data up to $p_{H_2O} = 300$ mbar, yielding $C_{w,01} = (99.9 \pm 7.5)$ ppm H_2O and $K_1 = (76 \pm 22)$ ppm⁻¹ bar⁻¹ with a correlation coefficient $r^2 = 0.84$. Second, $C_{w,01}$ was subtracted from the measured water contents, and data were fitted in the range from 0.5 to 15 bar. The obtained parameters for the second isotherm are $C_{w,02} = (113 \pm 63)$ ppm H_2O and $K_2 = (0.10 \pm 0.10)$ ppm⁻¹ bar⁻¹ with a correlation coefficient $r^2 = 0.77$. Although the Langmuir fit is of course only a rough approximation, it describes the trend of the data well. The similarity of K for plagioclase and K_2 for sanidine supports the idea that defects of type IIa OH are also present in sanidine.

Conclusion

A basic finding of this study is that the water content of igneous feldspars is not only dependent on water pressure, but also on the concentration of pre-existing defects in the feldspar. Such defects can be incorporated in the feldspars already during crystallization in the magma, but may have been formed also later by diffusion processes. In plagioclases, which are widely discussed as possible hygrometers for high-temperature magmas, especially vacancies on alkali sites may bound H_2O . Such V_{A1} vacancies can be formed by incorporation of an excess of silica in the feldspar structure as $V_{A1}Si_4O_8$ unit. Evidence for an excess of silica in high-temperature plagioclase is given by crystallization experiments along the join $CaAl_2Si_2O_8-SiO_2$ (Bruno and Facchinelli 1974; Ito 1976; Murakami et al. 1992), by analysis of plagioclases from lunar basalts (Beaty and Albee 1980), but also by tracer diffusion studies with labradorite single crystals (Behrens et al. 1990).

If one accepts that V_{A1} vacancies can host H_2O molecules in the feldspar structure, the term water solubility becomes another meaning. In this case, water solubility is not an intrinsic property of feldspars, but the water content is strongly affected by extrinsic defects in the feldspar structure. The consequence is that the use of plagioclases or other feldspars as hygrometers for magmas is rather difficult. In addition to an experimental determination of the water solubility in function of water fugacity and temperature, a determination of the concentration of the involved defects is needed for the feldspars in the natural sample. If the natural feldspar is of sufficiently good quality, the water solubility could be studied experimentally with it. However, this is very demanding and often the feldspar will not be suitable for such investigation. Only, if the vacancy concentration on A1 sites is not sensitive to the crystallization conditions, there is any chance to use it as a hygrometer.

Acknowledgements This paper is dedicated to Hans Wondratschek, whose passion was the sanidines from the Eifel. The sanidine SV was a donation from him, but I thank him also for numerous discussions in former times. The research was supported by the German Science foundation (DFG). Thanks to Dr. U. Reinholz from BAM, Berlin who performed the NRA measurements on the feldspars.

Funding Open Access funding enabled and organized by Projekt DEAL..

Open Access This article is licensed under a Creative Commons Attribution 4.0 International License, which permits use, sharing, adaptation, distribution and reproduction in any medium or format, as long as you give appropriate credit to the original author(s) and the source, provide a link to the Creative Commons licence, and indicate if changes were made. The images or other third party material in this article are included in the article's Creative Commons licence, unless indicated otherwise in a credit line to the material. If material is not included in the article's Creative Commons licence and your intended use is not permitted by statutory regulation or exceeds the permitted use, you will need to obtain permission directly from the copyright holder. To view a copy of this licence, visit <http://creativecommons.org/licenses/by/4.0/>.

References

- Aines RD, Rossman GR (1985) The high temperature behavior of trace hydrous components in silicate minerals. *Am Miner* 70:1167–1179
- Aines RD, Kirby SH, Rossman GR (1984) Hydrogen speciation in synthetic quartz. *Phys Chem Miners* 11:204–212
- Appleman DE, Nissen HU, Stewart DB, Clark JR, Dowty E, Huebner JS (1971) Studies of lunar plagioclases, tridymite, and cristobalite. *Geochim Cosmochim Acta Suppl* 2:117–133
- Baschek G, Johannes W (1995) The estimation of NaSi-CaAl interdiffusion rates in peristerites by homogenization experiments. *Eur J Miner* 7:295–307
- Beaty DW, Albee AL (1980) Silica solid solution and zoning in natural plagioclase. *Am Miner* 65:63–74

- Behrens H (1995) Determination of water solubilities in high-viscosity melts: an experimental study on $\text{NaAlSi}_3\text{O}_8$ and KAlSi_3O_8 melts. *Eur J Miner* 7:905–920
- Behrens H (2010) Ar, CO_2 and H_2O diffusion in silica glasses at 2 kbar pressure. *Chem Geol* 272:40–48
- Behrens H (2020) Water speciation in oxide glasses and melts. *Chem Geol* 558:119850
- Behrens H, Müller G (1995) An infrared spectroscopic study of hydrogen feldspar (HAlSi_3O_8). *Min Mag* 59:15–24
- Behrens H, Schmidt MO (1998) Infrared spectroscopy of hydrous silicic glasses at temperatures up to 600°C and implications for the incorporation and dynamics of water in the glasses. *N Jb Miner Abh* 172:203–226
- Behrens H, Johannes W, Schmalzried H (1990) On the mechanisms of cation diffusion processes in ternary feldspars. *Phys Chem Miner* 17:62–78
- Behrens H, Romano C, Nowak M, Holtz F, Dingwell DB (1996) Near-infrared spectroscopic determination of water species in glasses of the system $\text{MAAlSi}_3\text{O}_8$ (M = Li, Na, K): an interlaboratory study. *Chem Geol* 128:41–64
- Behrens H, Zhang Y, Leschik M, Wiedenbeck M, Heide G, Frischat GH (2007) Molecular H_2O as carrier for oxygen diffusion in hydrous silicate melts. *Earth Planet Sci Lett* 254:69–76
- Beran A (1986) A model of water allocation in alkali feldspar, derived from infrared-spectroscopic investigations. *Phys Chem Miner* 13:306–310
- Beran A (1987) OH Groups in nominally anhydrous framework structures: An infrared spectroscopic investigation of danburite and labradorite. *Phys Chem Miner* 14:441–445
- Bernotat-Wulf H, Bertelsmann D, Wondratschek H (1988) The annealing behaviour of Eifel sanidine (Volkesfeld): the influence of the sample surface and sample size on the order disorder transformation rate. *N Jb Miner Mh* 11:503–515
- Bertelmann D, Förtsch E, Wondratschek H (1985) On the annealing behaviour of sanidines: the exceptional case of Eifel sanidine megacrystals. *N Jb Miner Abh* 152:123–141 (**in German**)
- Bruno E, Facchinelli A (1974) Experimental studies on anorthite crystallization along the join $\text{CaAl}_2\text{Si}_2\text{O}_8\text{-SiO}_2$. *Bull Soc Fr Miner Cristallogr* 97:422–432
- Crank J (1975) The mathematics of diffusion, 2nd edn. Clarendon press, Oxford, p 414
- Derdau D, Freer R, Wright K (1998) Oxygen diffusion in anhydrous sanidine feldspar. *Contrib Miner Petrol* 133:199–204
- Doremus RH (1998) Comment on “Stationary and mobile hydrogen defects in potassium feldspar.” *Geochim Cosmochim Acta* 62:377–378
- Elphick SC, Graham CM, Dennis PF (1988) An ion microprobe study of anhydrous oxygen diffusion in anorthite: a comparison with hydrothermal data and some geological implications. *Contrib Miner Petrol* 100:490–495
- Farver JR (2010) Oxygen and hydrogen diffusion in minerals. *Rev Miner Geochem* 72:447–507
- Farver JR, Yund RA (1990) The effect of hydrogen, oxygen and water fugacity on oxygen diffusion in alkali feldspar. *Geochim Cosmochim Acta* 54:2953–2964
- Fehlmann M, Bertelmann D (1988) In situ synchrotron radiation topography of sanidines feldspars during annealing. In: Augustithis SS (ed) Synchrotron radiation applications in mineralogy and petrology. Theophrastus Publ, Athen, pp 205–216
- Freer R, Wright K, Kroll H, Göttlicher J (1997) Oxygen diffusion in sanidine feldspar and a critical appraisal of oxygen isotope-mass-effect measurements in non-cubic materials. *Phil Mag* A75:485–503
- Giletti BJ, Semet MP, Yund RA (1978) Studies in diffusion-III. oxygen in feldspars: an ion microprobe determination. *Geochim Cosmochim Acta* 42:45–57
- Goldsmith JR (1986) The role of hydrogen in promoting Al-Si interdiffusion in albite ($\text{NaAlSi}_3\text{O}_8$) at high pressures. *Earth Planet Sci Lett* 80:135–138
- Goldsmith JR (1987) Al/Si interdiffusion in albite: effect of pressure and the role of hydrogen. *Contrib Miner Petrol* 95:311–321
- Goldsmith JR (1988) Enhanced Al-Si diffusion in KAlSi_3O_8 at high pressures: the effect of hydrogen. *J Geol* 96:109–124
- Goldsmith JR (1991) Pressure-enhanced Al/Si diffusion and oxygen isotope exchange. In: Ganguly J (ed) Diffusion, atomic ordering and mass transport. *Adv Phys Geochem*, vol 8. Springer, New York, pp 221–247
- Graham CM, Elphick SC (1991) Some experimental constraints on the role of hydrogen in oxygen and hydrogen diffusion and Al-Si interdiffusion in silicates. In: Ganguly J (ed) Diffusion, atomic ordering and mass transport. *Adv Phys Geochem*, vol 8. Springer, New York, pp 248–285
- Grove TL, Baker MB, Kinzler RJ (1984) Coupled CaAl-NaSi diffusion in plagioclase feldspar: experiments and applications to cooling rate speedometry. *Geochim Cosmochim Acta* 48:2113–2121
- Hamada M, Kawamoto T, Takahashi E, Fujii T (2011) Polybaric degassing of island arc low-K tholeiitic basalt magma recorded by OH concentrations in Ca-rich plagioclase. *Earth Planet Sci Lett* 308:259–266
- Hamada M, Ushioda M, Fujii T, Takahashi E (2013) Hydrogen concentration in plagioclase as a hygrometer of arc basaltic melts: approaches from melt inclusion analyses and hydrous melting experiments. *Earth Planet Sci Lett* 365:253–262
- Hergemöller F, Wegner M, Deicher M, Wolf H, Brenner F, Hutter H, Abart R, Stolwijk NA (2017) Potassium self-diffusion in a K-rich single-crystal alkali feldspar. *Phys Chem Miner* 44:345–351
- Hofmeister AM, Rossman GR (1984) Determination of Fe^{3+} and Fe^{2+} concentrations in feldspar by optical absorption and EPR spectroscopy. *Phys Chem Miner* 11:213–224
- Hofmeister AM, Rossman GR (1985) A model for the irradiative coloration of smoky feldspar and the inhibiting influence of water. *Phys Chem Miner* 12:324–332
- Hui H, Peslier AH, Zhang Y, Neal CR (2013) Water in lunar anorthosites and evidence for a wet early Moon. *Nat Geosci* 6:177–180
- Ito J (1976) High temperature solvent growth of anorthite on the join $\text{CaAl}_2\text{Si}_2\text{O}_8\text{-SiO}_2$. *Contrib Miner Petrol* 59:187–194
- Johnson EA (2006) Water in nominally anhydrous crustal minerals: speciation, concentration, and geologic significance. *Rev Miner Geochem* 62:117–154
- Johnson EA, Rossman GR (2003) The concentration and speciation of hydrogen in feldspars using FTIR and ^1H MAS NMR spectroscopy. *Am Miner* 88:901–911
- Johnson EA, Rossman GR (2004) A survey of hydrous species and concentrations in igneous feldspars. *Am Miner* 89:586–600
- Johnson EA, Rossman GR (2013) The diffusion behavior of hydrogen in plagioclase feldspar at 800–1000 °C: implications for reequilibration of hydroxyl in volcanic phenocrysts. *Am Miner* 98:1779–1787
- Kats A (1962) Hydrogen in alpha quartz. *Phillips Res Repts* 17:1–31 (**133–195, 201–279**)
- Keppler H, Bagdasarov N (1993) High-temperature FTIR spectra of H_2O in rhyolitic melt to 1300°C. *Am Miner* 78:1324–1327
- Kohlstedt DL (2006) The role of water in high-temperature rock deformation. *Rev Miner Geochem* 62:377–396
- Kronenberg AK, Yund RA, Rossman GR (1996) Stationary and mobile hydrogen defects in potassium feldspar. *Geochim Cosmochim Acta* 60:4075–4094
- Kronenberg AK, Yund RA, Rossman GR (1998) Reply to the comment by Robert H. Doremus on “Stationary and mobile

- hydrogen defects in potassium feldspar." *Geochim Cosmochim Acta* 62:379–382
- Libowitzky E, Rossman GR (1996) Principles of quantitative absorbance measurements in anisotropic crystals. *Phys Chem Miner* 23:319–327
- Liu WD, Yang Y, Zhu KY, Xia QK (2018) Temperature dependences of hydrous species in feldspars. *Phys Chem Miner* 45:609–620
- McConnell JDC (1995) The role of water in oxygen isotope exchange in quartz. *Earth Planet Sci Lett* 136:97–107
- Mills RD, Simon JI, Alexander CMO'D, Wang J, Hauri EH (2017) Water in alkali feldspar: the effect of rhyolite generation on the lunar hydrogen budget. *Geochem Persp Lett* 3:115–123
- Mosenfelder JL, Rossman GR, Johnson EA (2015) Hydrous species in feldspars: a reassessment based on FTIR and SIMS. *Am Miner* 100:1209–1221
- Murakami H, Kimata M, Shimoda S, Ito E, Sasaki S (1992) Solubility of $\text{CaMgSi}_3\text{O}_8$ and Si_4O_8 endmembers in anorthite. *J Min Petr Econ Geol* 87:491–509
- Petrishcheva E, Rieder M, Predan J, Fischer FD, Giester G, Abart R (2018) Diffusion-controlled crack propagation in alkali feldspar. *Phys Chem Miner* 46:15–262
- Petrov I, Hafner SS (1988) Location of trace Fe^{3+} ions in sanidine, KAlSi_3O_8 . *Am Miner* 73:97–104
- Rossman GR (2006) Analytical methods for measuring water in nominally anhydrous minerals. *Rev Miner Geochem* 62:1–28
- Schuessler JA, Botcharnikov RE, Behrens H, Misiti V, Freda C (2008) Oxidation state of iron in hydrous phono-tephritic melts. *Am Miner* 93:1493–1504
- Seaman SJ, Dyar MD, Marinkovic N, Dunbar NW (2006) An FTIR study of hydrogen in anorthoclase and associated melt inclusions. *Am Miner* 91:12–20
- Shuai K, Yang X (2017) Quantitative analysis of H-species in anisotropic minerals by polarized infrared spectroscopy along three orthogonal directions. *Contrib Miner Petrol* 172:14
- Speit B, Lehmann G (1982) Radiation defects in feldspars. *Phys Chem Miner* 8:77–82
- Widder W, Wondratschek H, Fehlmann M, Klapper H (1994) X-ray topographic study of Eifel sanidine. *Z Kristallogr* 209:206–209
- Wilangowski F, Abart R, Divinski SV, Stolwijk NA (2015) Radiotracer experiments and Monte Carlo simulations of sodium diffusion in alkali Feldspar: evidence against the vacancy mechanism. *Defect Diffus Forum* 363:79–84
- Yang X (2012) An experimental study of H solubility in feldspars: effect of composition, oxygen fugacity, temperature and pressure and implications for crustal processes. *Geochim Cosmochim Acta* 97:46–57
- Yang X, Keppler H, McCammon C, Ni H (2012) Electrical conductivity of orthopyroxene and plagioclase in the lower crust. *Contrib Miner Petrol* 163:33–48
- Yund RA (1986) Interdiffusion of NaSi–CaAl in Peristerite. *Phys Chem Miner* 13:11–16
- Yund RA, Anderson TF (1974) The effect of fluid pressure on oxygen isotope exchange between feldspar and water. *Geochim Cosmochim Acta* 42:235–239
- Yund RA, Tullis J (1980) The effect of water, pressure and strain on Al/Si order-disorder kinetics in feldspar. *Contrib Miner Petrol* 72:297–302
- Zarubin DP (2000) Modelling the OH stretch envelope shape and temperature effects in infrared spectra of hydrous silica and silicate glasses. *Phys Chem Miner* 27:590–597
- Zhang Y, Stolper EM, Wasserburg GJ (1991) Diffusion of a multi-species component and its role in oxygen and water transport in silicates. *Earth Planet Sci Lett* 103:228–240
- Zhang B, Shan S, Wu X (2016) H, Na, and K diffusion in plagioclase feldspar by relating point defect parameters to bulk properties. *Phys Chem Miner* 43:151–159

Publisher's Note Springer Nature remains neutral with regard to jurisdictional claims in published maps and institutional affiliations.